Earth Surface Processes and Landforms
Earth Surf. Process. Landforms **33**, 1129–1151 (2008)
Published online in Wiley InterScience
(www.interscience.wiley.com) **DOI:** 10.1002/esp.1689

Implications of the Saltation–Abrasion Bedrock Incision Model for Steady-State River Longitudinal Profile Relief and Concavity

Leonard S. Sklar[1]* and William E. Dietrich[2]
[1] *Department of Geosciences, San Francisco State University, San Francisco, CA, USA*
[2] *Department of Earth and Planetary Science, University of California, Berkeley, CA, USA*

**Correspondence to: Leonard S. Sklar, Department of Geosciences, San Francisco State University, 1600 Holloway Avenue, San Francisco, CA 94132, USA.*

Received 30 April 2006;
Revised 28 December 2007;
Accepted 3 March 2008

Abstract

The saltation–abrasion model predicts rates of river incision into bedrock as an explicit function of sediment supply, grain size, boundary shear stress and rock strength. Here we use this experimentally calibrated model to explore the controls on river longitudinal profile concavity and relief for the simple but illustrative case of steady-state topography. Over a wide range of rock uplift rates we find a characteristic downstream trend, in which upstream reaches are close to the threshold of sediment motion with large extents of bedrock exposure in the channel bed, while downstream reaches have higher excess shear stresses and lesser extents of bedrock exposure. Profile concavity is most sensitive to spatial gradients in runoff and the rate of downstream sediment fining. Concavity is also sensitive to the supply rate of coarse sediment, which varies with rock uplift rate and with the fraction of the total sediment load in the bedload size class. Variations in rock strength have little influence on profile concavity. Profile relief is most sensitive to grain size and amount of runoff. Rock uplift rate and rock strength influence relief most strongly for high rates of rock uplift. Analysis of potential covariation of grain size with rock uplift rate and rock strength suggests that the influence of these variables on profile form could occur in large part through their influence on grain size. Similarly, covariation between grain size and the fraction of sediment load in the bedload size class provides another indirect avenue for rock uplift and strength to influence profile form. Copyright © 2008 John Wiley & Sons, Ltd.

Keywords: river profile; bedrock channels; erosion; sediment supply; geomorphology

Introduction

The decline in river channel slope with increasing drainage area, which results in a concave-up profile form, is a typical and fundamental characteristic of tectonically active landscapes. River profile concavity has been explained previously in terms of alluvial river characteristics, such as downstream fining of bed material size, downstream accumulation of water and sediment from tributary inputs, and river interaction with coastal boundary conditions (Mackin, 1948; Hack, 1957; Brush, 1961; Snow and Slingerland, 1987; Sinha and Parker, 1996; Rice and Church, 2001). River profile concavity has also been used in the context of bedrock channels to motivate or parameterize simple bedrock incision models, such as the stream power model, under the assumption that there is an 'intrinsic' steady state profile concavity that is an expression of the underlying physics of bedrock erosion (Seidl *et al.*, 1994; Stock and Montgomery, 1999; Whipple and Tucker, 1999; Whipple, 2001; Kirby and Whipple, 2001; Roe *et al.*, 2002; Tucker and Whipple, 2002).

The saltation–abrasion model (Sklar *et al.*, 1996; Sklar and Dietrich, 1998, 2001, 2004, 2006) provides an alternative approach to understanding river longitudinal form because it directly couples the mechanics of sediment transport and bedrock incision, in effect merging the alluvial and bedrock channel perspectives. We focus on the role of bedload in bedrock incision because bedload sediment transport is ubiquitous in bedrock channels, bedload impacts are an efficient mechanism for transferring energy from the flow to the bedrock bed and transient deposits of alluvium can bury portions of the bed and insulate underlying bedrock from the erosive forces of the flow. In previous contributions

we have derived this model for river incision by saltating bedload and constrained all parameters values with experimental data (Sklar and Dietrich, 1998, 2001, 2004). We have also developed a method for scaling the model up from the temporal and spatial scale of individual grain impacts, at which it was derived, to the scale at which landscapes evolve, and explored the model predictions for the controls on steady-state channel slope (Sklar and Dietrich, 2006). Here we extend the analysis to the drainage basin scale to explore the model's implications for understanding the controls on steady-state river longitudinal profile concavity and relief.

We focus on the simple illustrative case of topographic steady state, in which the rate of vertical rock uplift is equal to the rate of channel incision, because we can most clearly explore the sensitivity of model predictions of profile form to variations in the independent variables, such as discharge, rock strength and rock uplift rate. Steady state is also a reference state against which to detect the signal of transients in landscape evolution. Note that steady-state topography represents one of several examples of the more general case of a spatially uniform erosion rate. Understanding the steady-state predictions of geomorphic process rate models is an essential step even if true topographic steady state is unlikely to be achieved in most tectonically active landscapes (Whipple, 2001; Willett and Brandon, 2002), and is necessary to properly interpret comparisons among models simulating transient landscapes (e.g. Hancock and Willgoose, 2002; Tucker and Whipple, 2002; van der Beek and Bishop, 2003).

Sediment-flux dependent incision models have been used previously to explore the controls on longitudinal profile form, in both steady state and transient contexts (Howard *et al.*, 1994; Kooi and Beaumont, 1996; Sklar and Dietrich, 1998; Whipple and Tucker, 2002; van der Beek and Bishop, 2003; Gasparini *et al.*, 2006). The work reported here is unique in several respects. Unlike other model formulations, the saltation–abrasion model explicitly accounts for the role of grain size in controlling erosional efficiency and steady-state channel slope (Sklar and Dietrich, 2006). Moreover, we conduct a comprehensive sensitivity analysis and investigate several key potential linkages among the variables that together control river longitudinal profile form.

Profile concavity is typically quantified assuming a power law scaling between channel slope S and drainage area A

$$S = k_s A^{-\Theta} \tag{1}$$

where the values of the coefficient k_s and exponent Θ are determined by log–log linear least squares regression (see, e.g., Hack, 1957; Flint, 1974; Kirby and Whipple, 2001). Larger values of Θ correspond to a more rapid decline in slope with drainage area, and therefore to greater profile concavity. Much debate has surrounded the expected value of Θ, which can be derived for the case of steady-state topography from simple scaling arguments for patterns of energy expenditure (see, e.g., Rodriguez-Iturbe and Rinaldo, 1997) or for controls on rates of bedrock incision (see, e.g., Howard and Kerby, 1983; Seidl and Dietrich, 1992). These scaling arguments typically predict $0{\cdot}35 < \Theta < 0{\cdot}5$, and although values in this range are often observed it is also common to find values of Θ outside this range, including $\Theta = 1{\cdot}0$ or greater (see, e.g., Hack, 1957; Brush, 1961; Sklar and Dietrich, 1998; Montgomery and Lopez-Blanco, 2003).

Empirical analysis of river profile slope–area scaling is complicated by two important considerations. First, the observed log–log linear relationship does not hold for steeper headwater channel slopes, where debris flow scour is inferred to be the dominant erosional process (Montgomery and Foufoula-Georgiou, 1993; Sklar and Dietrich, 1998; Stock and Dietrich, 2003). The relationship between slope and area, plotted in log–log space, appears to be curved rather than linear, for channels steeper than about 5–20 percent, and with drainage areas smaller than ~1 km^2 (Stock and Dietrich, 2003). As a result, log–log linear regressions of slope with drainage area that include regions dominated by both fluvial and debris flow processes tend to systematically under-estimate the concavity of the fluvial portion of the profile. Second, profiles that are clearly not in topographic steady state, for example where a transient wave of incision is sweeping upstream, will nonetheless often exhibit log–log linear slope–area scaling (Hack, 1965; Sklar and Dietrich, 1998). Even where approximate topographic steady state can be demonstrated (Willett and Brandon, 2002), slope–area scaling may not provide a diagnostic test to determine the most appropriate model for bedrock incision due to the problem of equifinality (Bevin, 1996). As van der Beek and Bishop (2003) have shown, similar expected profile concavities can be derived from widely differing assumptions.

Unlike bedrock incision models based on simple scaling arguments, the saltation–abrasion model was derived without any *a priori* expectation that it would predict any particular concavity or even log–log linear slope–area scaling for steady-state river profiles. Because the effects of sediment supply, grain size and rock strength, along with channel slope, discharge, and channel roughness and cross-sectional geometry, are explicitly represented in the saltation–abrasion model, it may provide more detailed, physically based explanations for the commonly observed decline of channel slope with increasing drainage area.

Predictions of steady-state river profiles using the saltation–abrasion model can also be used to consider the controls on river profile relief. Relief is perhaps the most fundamental landscape attribute, and for more than a century geomorphologists have debated the relative importance of factors such as climate, rock strength and rock uplift rate in

DOI: 10.1002/esp

setting landscape relief (e.g. Gilbert, 1877; Ahnert, 1970; Molnar and England, 1990). All else equal, greater relief is typically expected for stronger rocks, more rapid rates of rock uplift and drier climates, although the role of climate is the subject of considerable debate (see, e.g., Molnar, 2001). Consideration of the role of sediment supply and grain size in controlling rates of bedrock incision (Sklar and Dietrich, 1998, 2001, 2004), however, suggests that profile relief may be less sensitive to spatial or temporal variations in climate, rock strength or rates of rock uplift than has been predicted by studies using the stream power bedrock incision model (e.g. Whipple and Tucker, 1999; Kirby and Whipple, 2001).

Here we use the saltation–abrasion model to generate a large suite of predicted steady-state river profiles, in order to evaluate the relative influence of each of the key variables (discharge, grain size, sediment supply, rock uplift rate and rock strength) in controlling profile concavity and profile relief. We begin by briefly reviewing the model development, and then introduce an analytical framework for distinguishing the relative contributions of grain size, sediment supply, rock uplift rate and rock strength rate to the total shear stress required for steady state at any given point along the river profile. Next we consider in detail a representative steady-state profile, to illuminate under what conditions the model predicts approximately log–log linear slope–area scaling and provide a template for understanding the model behavior in the subsequent sensitivity analysis. We then explore the sensitivity of profile concavity and relief to variations in the key variables, treating each as independent. We conclude by considering some of the possible covariation of key variables, in particular the likely dependence of grain size on both rock uplift rate and rock strength.

Model overview

The saltation–abrasion model predicts an instantaneous rate of bedrock incision (E_i) as a function of the representative sediment grain size (D_s), the supply rate of coarse sediment (Q_s), rock tensile strength (σ_T), water discharge (Q_w), channel width (W), slope and channel roughness (Sklar and Dietrich, 2004). The model is based on the idea that incision rate can be treated as the product of three terms: the average volume of rock removed by an individual bedload impact (V_i), the impact rate per unit time per unit bed area (I_r) and the fraction of the bed not armored by transient deposits of alluvium and thus composed of exposed bedrock (F_e),

$$E_i = V_i I_r F_e \tag{2}$$

Expressions for each of these three terms are obtained from empirical studies of impact wear (Bitter, 1963; Head and Harr, 1970) and saltation trajectories (e.g. Abbott and Francis, 1977; Hu and Hui, 1996), from experiments using bedrock abrasion mills (Sklar and Dietrich, 2001) and by assuming that the extent of bed exposure depends on the ratio of sediment supply to sediment transport capacity (Q_t)

$$F_e = 1 - Q_s/Q_t \tag{3}$$

for $Q_s/Q_t < 1$; $F_e = 0$ when $Q_s/Q_t \geq 1$.

We then rewrite Equation (2) as

$$E_i = \frac{0{\cdot}08 R_b g Y}{k_v \sigma_T^2} \frac{Q_s}{W} \left(\frac{\tau^*}{\tau_c^*} - 1 \right)^{-0{\cdot}52} \left(1 - \frac{Q_s}{Q_t} \right) \left(1 - \left(\frac{u^*}{w_f} \right)^2 \right)^{3/2} \tag{4}$$

where R_b is the non-dimensional buoyant density ($R_b = (\rho_s - \rho_w)/\rho_w$), ρ_s and ρ_w are the densities of sediment and water respectively, g is the gravitational acceleration, Y is the rock modulus of elasticity, σ_T is the rock tensile strength and k_v is a dimensionless parameter that represents the impact kinetic energy required to detach a unit volume per unit rock tensile strength (experiments indicate that $k_v \approx 10^6$, reported as 10^{12} J m^{-3} MPa^{-1} by Sklar and Dietrich, 2004). In Equation (4), u^* is the shear velocity ($u^* = (gR_hS)^{1/2}$) and w_f is the grain fall velocity in still water, τ^* is the non-dimensional shear stress

$$\tau^* = R_h S / R_b D_s \tag{5}$$

where R_h is the hydraulic radius, S is the channel slope, D_s is the representative sediment grain diameter and τ_c^* is the value of τ^* at the threshold of sediment motion. We calculate the bedload sediment transport capacity Q_t using the expression of Fernandez-Luque and van Beek (1976)

$$Q_t = 5{\cdot}7 \rho_s W (R_b g D_s^3)^{1/2} (\tau^* - \tau_c^*)^{3/2} \tag{6},$$

DOI: 10.1002/esp

although similar results would be obtained with most other bedload transport relations because they have a similar dependence on excess shear stress (see the review by Gomez and Church, 1989).

In scaling the model up in time, from individual bedload impacts to river profile evolution, we assume that all transport of coarse sediment and incision into bedrock takes place during a representative high-flow discharge, which occurs only during some fraction of total time (F_t) (Sklar and Dietrich, 2006). A low-flow discharge insufficient to mobilize bedload is assumed to occur during the remaining time ($1 - F_t$); together, the high and low discharges pass the total annual volume of runoff while the total annual flux of bedload moves only during the high flow discharge. Here we use a value of $F_t = 0{\cdot}0437$, to be consistent with the magnitude-frequency analysis described in detail by Sklar and Dietrich (2006).

At topographic steady state, the rock uplift rate (U_r) is equal to the long-term incision rate ($E_{lt} = E_i F_t$), and the coarse sediment supply rate can be expressed as

$$Q_s = \frac{\rho_s E_{lt} A F_{bl}}{F_t} \tag{7}$$

where F_{bl} is the coarse fraction of the total sediment load that moves as bedload. To scale up in space from the reach to the profile scale (Sklar and Dietrich, 2006), we treat width and discharge as power functions of drainage area A,

$$Q_w = bA^p \tag{8}$$

$$W = cQ_w^f = bcA^{fp} \tag{9}$$

where b, c, p and f are empirical parameters, and let drainage area and grain size vary as power functions of distance downstream of the channel head (x),

$$A = A_0 + dx^h \tag{10}$$

$$D_s = D_0[(x + x_0)/x_0]^{-\alpha} \tag{11}$$

where A_0 and D_0 are the drainage area and grain size at the channel head and x_0 is the unchanneled distance from the drainage divide to the channel head.

Analytical Framework

For topographic steady state to occur, the rate of rock uplift must be balanced by the rate of bedrock incision everywhere along the river profile. At any given point along the profile, sufficient shear stress must be available to accomplish three things, listed here in order of increasing shear stress required: mobilize coarse sediment on the channel bed, transport coarse sediment at the rate of supply from upstream and erode bedrock at the rate of rock uplift. Thus, the total average boundary shear stress τ_T can be considered to be a sum of three components,

$$\tau_T = \tau_D + \Delta\tau_{Qs} + \Delta\tau_E \tag{12}$$

where τ_D is the shear stress required to initiate grain motion, $\Delta\tau_{Qs}$ is an additional increment of shear stress required to transport the bedload at the rate of supply from upstream and $\Delta\tau_E$ is another increment of shear stress required to erode bedrock at the rate of rock uplift. Analytical expressions for the first two shear stress components can be obtained by rearranging Equation (6):

$$\tau_D = (\rho_s - \rho_w) g D_s \tau_c^* \tag{13}$$

$$\Delta\tau_{Qs} = \left(\frac{Q_s g (\rho_s - \rho_w)^{3/2}}{5{\cdot}7 W \rho_s R_b^{1/2}} \right)^{2/3} \tag{14}$$

The marginal increase in shear stress required to erode bedrock by saltating bedload impacts, $\Delta\tau_E$, cannot be expressed explicitly by rearranging Equation (4); rather, it must be solved for numerically. For steady state conditions, $\Delta\tau_E$ will depend principally on rock uplift rate, rock strength and grain size:

DOI: 10.1002/esp

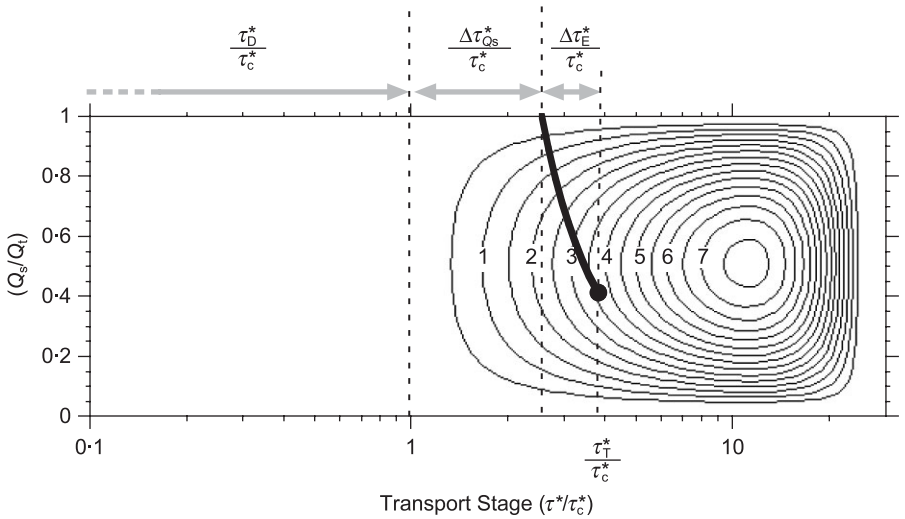

Figure 1. Definition plot for the partitioning of the total shear stress into three components ($\tau_T = \tau_D + \Delta\tau_{Qs} + \Delta\tau_E$), utilizing the non-dimensional representation of the saltation–abrasion model. Shear stress is expressed as the non-dimensional Shields stress ($\tau^* = \tau/(\rho_s - \rho_w)gD_s$). The dimensionless bedrock incision rate ($E^* = E_i\sigma_T^2/\rho_s Y(gD_s)^{3/2}$; labeled contours, axis out of page) is a function of transport stage (τ^*/τ_c^*) and relative sediment supply (Q_s/Q_t). For $\tau_T \leq (\tau_D + \Delta\tau_{Qs})$, the bed is assumed to be fully alluviated and no bedrock incision can occur ($\Delta\tau_E = 0$). The heavy line shows the plotting position of an example channel reach as τ_T is increased above $\tau_D + \Delta\tau_{Qs}$ (i.e. $\Delta\tau_E > 0$), for the case where $Q_s = 160$ kg/s, with slope varying from 0·011 to 0·019 (all other variables held constant; see Table I). Note that although the channel reach plotting position will shift for different input values (e.g. sediment supply or grain size), the contours define a unique functional surface valid for all physically reasonable values of discharge, channel width, slope, sediment supply, grain size, channel roughness and rock strength.

$$\Delta\tau_E = f(U_r,\ \sigma_T,\ D_s) \tag{15}$$

The three shear stress component terms of Equation (12) can be depicted graphically, using the non-dimensional contour map of the saltation–abrasion model functional surface introduced previously (Sklar and Dietrich, 2004, Figure 16 therein). In this framework, predicted incision rate collapses to a unique functional surface, the height of which depends on transport stage (τ^*/τ_c^*) and relative supply rate (Q_s/Q_t) for all physically reasonable combinations of discharge, slope, width, grain size, sediment supply, channel roughness and rock strength. Figure 1 shows the saltation–abrasion incision function plotted as contours of constant dimensionless incision rate (E^*) in which incision has been non-dimensionalized by rock tensile strength (σ_T) and grain size (D_s), such that $E^* = E_i\sigma_T^2/\rho_s Y(gD_s)^{3/2}$. At the threshold of grain motion $\tau_T = \tau_D$, but $E_i = 0$ because the bed is assumed to be fully alluviated. Increasing the shear stress by the increment $\Delta\tau_{Qs}$ provides sufficient stress to transport the load supplied from upstream; however, when $\tau_T = \tau_D + \Delta\tau_{Qs}$ the bed remains fully alluviated and $E_i = 0$. The dark line in Figure 1 shows the plotting position of an example channel reach as τ_T is increased above $\tau_D + \Delta\tau_{Qs}$ (i.e. $\Delta\tau_E > 0$), for the case where $Q_s = 160$ kg/s, $D_s = 0{\cdot}06$ m, $W = 18$ m and $\sigma_T = 7$ MPa. Increasing the shear stress (for example by increasing the channel slope) by the additional increment $\Delta\tau_E$ exposes a fraction of the channel bed, as reflected in the downward shift of the plotting position of the channel reach with respect to the relative supply axis, allowing incision to occur. The channel plotting position moves to higher incision rate contours as transport stage increases, due to the increasing extent of bedrock exposure and the increasing grain impact energy.

Decomposing the total shear stress into these three components is useful for understanding the variation in shear stress along the length of the steady-state profile. For example, consider the idealized case of spatially uniform rock uplift and spatially uniform total shear stress, as would be expected if incision rate were a simple power function of shear stress (see, e.g., Howard, 1994; Whipple and Tucker, 1999). The downstream increase in sediment supply, due to increasing drainage area, results in a linear increase in the magnitude of the transport stress increment $\Delta\tau_{Qs}$ with drainage area. Neglecting for the moment any downstream variation in bedrock incision stress increment $\Delta\tau_E$, for the total shear stress τ_T to remain constant along the profile the grain size must decline, such that the decrease in the threshold of motion stress τ_D offsets the increase in $\Delta\tau_{Qs}$.

DOI: 10.1002/esp

Example Steady-state Profile

In this section we describe an example steady-state profile to illustrate how downstream variations in many of the input variables to the saltation–abrasion model give rise to the predicted long profile concavity and relief. Because the sensitivity analysis that follows this section necessarily involves the prediction of hundreds of profiles, it is not feasible to provide a detailed account of the internal behavior of the model for each profile. Therefore, the following detailed examination of a single profile is intended to serve as a template for understanding how changes to input variable and parameter values translate into changes in predicted steady-state profile concavity and relief.

For this example we use physically reasonable values for the watershed scaling parameters (listed in Table I), which were selected so that the predicted steady-state profile passes through a reference field site on the South Fork Eel River, in Northern California. As in the previous papers describing the model development and testing (Sklar and Dietrich, 2004, 2006), we use the reference site as a field anchor point for appreciating how widely we vary the value of the various model variables and parameters in the sensitivity analysis below. For simplicity, in this example we assume that rock uplift rate, rock strength and channel roughness are spatially uniform. We also assume that runoff is spatially uniform ($p = 1{\cdot}0$), and that the fraction of total load in the bedload size class (F_{bl}) is constant along the profile.

Figure 2(a) shows the steady-state river longitudinal profile predicted by the saltation–abrasion model, for the watershed scaling parameters listed in Table I. The profile has a concave-up form, and profile relief is roughly 600 m over the 100 km distance between headwaters and downstream boundary. The location of the S. Fork Eel reference site is marked by the open circle. The example profile exhibits approximately log–log linear scaling between channel

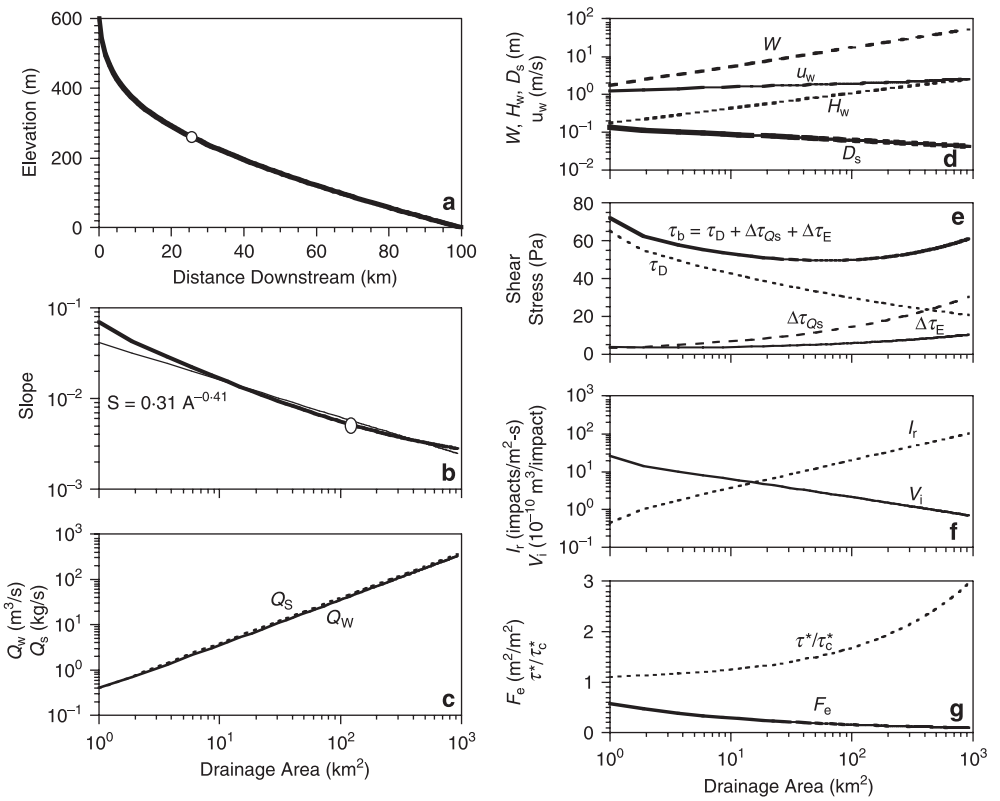

Figure 2. Example steady-state profile predicted by saltation–abrasion model for variable and parameter values listed in Table I. (a) Change in channel bed elevation with distance; open circle indicates S. Fork Eel River reference site. (b) Variation in channel slope with drainage area, showing model prediction (heavy line) and best-fit log–log linear regression line. (c) Variation in discharge Q_w and coarse sediment supply Q_s with drainage area. (d) Variation in channel width W, flow depth H_w, grain diameter D_s and flow velocity u_w with drainage area. (e) Variation in total shear stress τ_T and shear stress components responsible for initiation of sediment motion τ_D, transport of supplied coarse sediment load $\Delta\tau_{Qs}$ and bedrock erosion $\Delta\tau_E$. (f) Variation in bedload particle impact rate I_r and volume of rock eroded per impact V_i with drainage area. (g) Variation in transport stage τ^*/τ_c^* and fraction of bed composed of bedrock exposures F_e with drainage area.

DOI: 10.1002/esp

Table I. Example steady-state profile model parameters

Unchanneled area	$A_0 = 1\ \text{km}^2$
Unchanneled length	$L_0 = 1\ \text{km}$
Area length exponent	$h = 1{\cdot}5$
Area length coeff.	$d = 30\ \text{km}^{2-h}$
High flow time fraction	$F_t = 0{\cdot}0437$
Discharge area exponent	$p = 1{\cdot}0$
Discharge area coeff.	$b = 0{\cdot}347\ \text{m}^3\ \text{s}^{-1}\ \text{km}^{-2p}$
Width discharge exponent	$f = 0{\cdot}5$
Width discharge coeff.	$c = 3{\cdot}0\ \text{m}^{1-3f}\ \text{s}^f$
Downstream fining exponent	$\alpha = 0{\cdot}25$
Channel head grain size	$D_0 = 0{\cdot}134\ \text{m}$
Bedload supply fraction	$F_{bl} = 0{\cdot}22$
Rock uplift rate	$U_r = 0{\cdot}9\ \text{mm yr}^{-1}$
Rock tensile strength	$\sigma_T = 7\ \text{MPa}$
Critical shear stress	$\tau_c^* = 0.03$
Mannings roughness coeff.	$n = 0{\cdot}035\ \text{m}^{-1/3}\ \text{s}$

slope and drainage area, with $\Theta = 0{\cdot}41$ ($R^2 = 0{\cdot}974$), as shown in Figure 2(b). However, there is clear structure in the residuals, due to a weakly concave-up curvature to the log–log plot of slope with drainage area.

To understand why the model predicts approximately log–log linear slope area scaling, and also why the predicted profile deviates systematically from log–log linear scaling, it is helpful to consider the spatial variation in the input variables and in the hydraulic quantities calculated within the model. In the process we can also verify that the model predicts physically reasonable and mutually consistent values for these intermediate quantities.

As shown in Figure 2(c), both sediment supply (Q_s) and discharge (Q_w) increase linearly with drainage area. Figure 2(d) shows the downstream variation in channel width (W), flow depth (H_w) and flow velocity (u_w), as well as grain diameter (D_s). For this example, we have chosen a relatively rapid rate of downstream fining of grain size ($\alpha = 0{\cdot}25$). To be consistent with the mechanistic assumptions underlying the model, the range of grain sizes, and thus the potential rate of fining, is constrained by the requirements that flow depth exceeds grain diameter and that particle Reynolds numbers remain in the hydraulically rough regime (Sklar and Dietrich, 2004).

Figure 2(e) shows the downstream variation in total shear stress (τ_T), as well as in the three stress component terms (τ_D, $\Delta\tau_{Qs}$ and $\Delta\tau_E$). To first order, the predicted profile concavity is due to the nearly constant total shear stress required to incise at the rate of rock uplift. The downstream increase in flow depth of about an order of magnitude is compensated for by a downstream decrease in channel slope of similar magnitude. However, the relative influence of each of the component shear stress terms is not constant along the profile, and it is the variation in the sum of these components that gives rise to the deviation from exact power law slope–area scaling.

In the upstream reaches, the total shear stress is dominated by τ_D, the shear stress required to initiate grain motion. Only small increments of shear stress are required to transport the load of coarse sediment and expose sufficient bedrock to erode at the rate of rock uplift. With increasing drainage area, τ_D declines steadily due to the fining of the representative coarse grain size, but remains the dominant shear stress component through the majority of the profile length.

The downstream reduction in τ_D is offset by the downstream increases in $\Delta\tau_{Qs}$ and $\Delta\tau_E$, which occur primarily because of the increase in coarse sediment supply with increasing drainage area. Because sediment supply grows linearly with area, while channel width only increases as the square root of area (for the parameter values used here), the stress in excess of the threshold of motion ($\Delta\tau_{Qs}$) must increase to accommodate the increased load per unit width. The downstream increase in $\Delta\tau_E$ occurs because, as sediment supply increases, greater shear stresses are required to expose sufficient bedrock to achieve the same rate of bedrock wear. The downstream variation in $\Delta\tau_E$ is best understood by considering the predicted frequency and efficiency of bedload impacts with exposed bedrock predicted by the model.

Figure 2(f), (g) shows the downstream variations in the three fundamental terms of the saltation–abrasion model, the volume of rock eroded per unit impact (V_i), the impact rate per unit area per unit time (I_r) and the fraction of the bed exposed (F_e). The derivation of the saltation–abrasion model is based on the assumption that bedrock erosion rate can be expressed as the product of these three terms. From upstream to downstream, there is a shift in the erosive magnitude and frequency of bedload impacts. Upstream, where grain diameters are largest but sediment supply per unit width is lowest, bedrock wear is dominated by relatively infrequent (low I_r) but highly erosive (high V_i) bedload impacts. Moving downstream, impact frequency increases while erosive efficiency decreases, due to the decrease in

DOI: 10.1002/esp

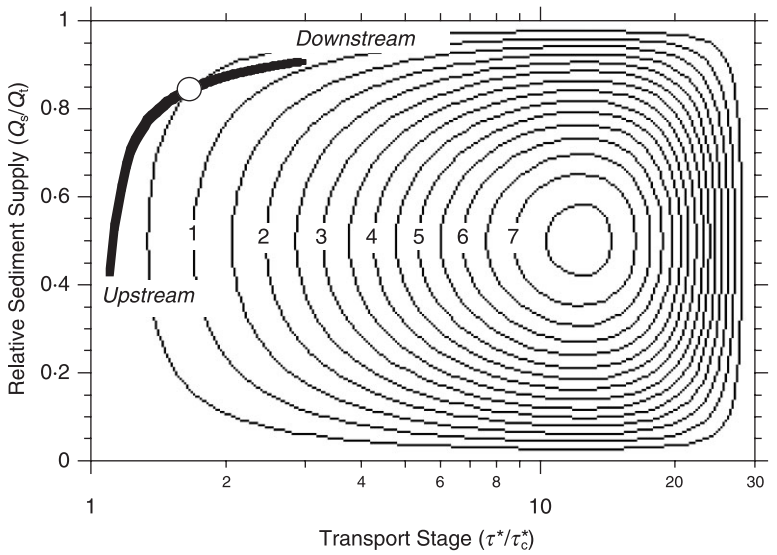

Figure 3. Example steady-state profile plotted on non-dimensional functional surface of saltation–abrasion model (Figure 1). Open circle indicates field reference site.

grain size and the increase in sediment supply. Overall, the rate at which exposed bedrock is eroded increases downstream, because I_r grows faster than V_i declines. This effect is compensated for by a downstream decrease in the fraction of the bed that is exposed to abrasive wear, so that fewer bedload impacts strike exposed bedrock, thus maintaining a uniform incision rate along the length of the profile.

The example steady-state profile is dominated by a transition from a coarse, weakly mobile bed with extensive bedrock exposure in the upstream reaches, to a finer, highly mobile bed with limited bedrock exposure in the downstream reaches. The change in relative mobility is shown in Figure 2(g) by the downstream increase in transport stage (τ^*/τ_c^*), which occurs primarily because of the decline in grain size. This downstream transition in the channel condition is perhaps better illustrated in the context of the non-dimensional contour map of the saltation–abrasion functional surface, as shown in Figure 3. Moving from upstream to downstream, the plot of the example steady-state profile curves away from the threshold of motion, and toward the condition of full alluviation. Note that the S. Fork Eel River reference site is plotted as an open circle. Note also that, although the incision rate is spatially uniform, the profile does not follow a contour, because incision rate is non-dimensionalized by grain size, which changes along the profile ($E^* = E_i\sigma_T^2/\rho_s Y(gD_s)^{3/2}$).

The steady-state profiles generated for the sensitivity analysis in the following sections follow the same general trend of downstream transitions in transport stage and bed exposure as demonstrated by this example profile. However, within this overall pattern, large differences in profile concavity and relief can occur due to changes in the magnitude and spatial variation of the key input variables of discharge, grain size, sediment supply, rock uplift rate and rock strength. An exhaustive sensitivity analysis, in which the magnitude and spatial variation of each variable is tested independently, is beyond the scope of this study. Rather, we attempt to chart a course through the parameter space that identifies the relative importance of each of these variables in influencing profile concavity and relief. Our strategy is to follow the hierarchy of influences suggested by the three components of total shear stress discussed in the previous section. Accordingly, the sensitivity analysis begins with conditions favoring a dominant control by grain size, then sediment supply and finally rock wear.

Sensitivity Analysis

The influence of discharge

Discharge influences incision rate through the contribution of flow depth to the total shear stress available to move sediment and erode rock. All else equal, larger discharges result in less steep steady-state channel slopes. Therefore, we commonly expect lower relief in wetter climates and less profile concavity where orographic effects concentrate

DOI: 10.1002/esp

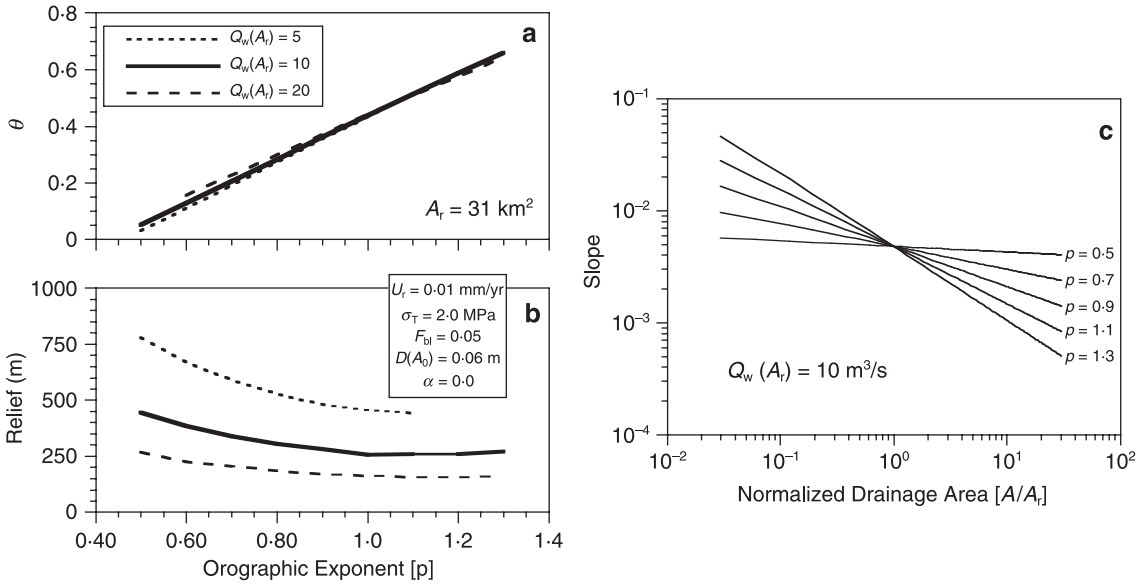

Figure 4. Influence of discharge on steady-state profile form. Variation in slope–area scaling exponent Θ (a) and profile relief (b) with orographic exponent p, for various magnitudes of basin-average runoff represented by the discharge at a representative drainage area $Q_w(A_r)$. (c) Variation in channel slope with drainage area for various values of p, illustrating the effect of normalizing drainage area by A_r. Constant values of variables and parameters not varied indicated in figure or as listed in Table I.

rainfall in the upstream portions of the drainage basin (Roe *et al.*, 2002). Steady-state profiles predicted by the saltation–abrasion model are consistent with these expectations, and provide a quantitative estimate of the degree of sensitivity of profile form to the magnitude and spatial variation in discharge.

The influence of discharge on profile form is most clearly seen when the total shear stress required to maintain steady state is approximately spatially uniform, thus highlighting the tradeoff between discharge and slope in generating shear stress. As can be inferred from the preceding discussion of the example steady-state profile, if grain size is constant along the profile ($\alpha = 0$) then total shear stress must increase downstream to accommodate the increase in sediment supply per unit width. However, if the uniform grain size is large, and the sediment supply low, then the total shear stress (τ_T) will be dominated by the constant threshold of motion stress component (τ_D) throughout the length of the profile, and the downstream increase in transport stress increment $\Delta\tau_{Qs}$ will not generate a significant variation in τ_T. These conditions are obtained for low values of rock uplift rate (U_r), rock strength (σ_T) and fraction of total sediment load that moves as bedload (F_{bl}).

Figure 4(a) shows the variation in the slope–area scaling exponent Θ for different values of the exponent p, the parameter that controls the spatial distribution of runoff along the profile (Equation (8)). Low values of p could correspond to strong orographic effects, with rainfall concentrated in the higher elevation headwaters of the drainage basin; values of $p > 1{\cdot}0$ occur when rainfall is greater in the lower elevation downstream reaches of the channel network. Note that the exponent p can also vary due to hydrologic effects such as storm size and duration relative to basin size and flood peak travel time (O'Connor and Costa, 2004). As demonstrated by Figure 4(a), downstream variations in runoff can have a profound influence on profile concavity. When the orographic effect is particularly strong ($p < 0{\cdot}5$) the steady-state profile may become nearly planar ($\Theta \approx 0{\cdot}0$).

In contrast, variations in the basin-average runoff have little influence on profile concavity (Figure 4(a)), but do strongly influence profile relief (Figure 4(b)). To represent changes in average runoff we use the discharge at a representative drainage area $Q_w(A_r)$, where A_r is the midpoint in the range of log-transformed drainage areas,

$$A_r = \frac{[\log(A_L) - \log(A_0)]}{2} \tag{16}$$

and A_L and A_0 are the drainage areas at the downstream and upstream ends of the profile respectively. The advantage of this approach is that A_r is the only location along the profile where changes in the orographic exponent p have no effect on the magnitude of the discharge. Thus the predicted steady-state channel slope at A_r is unaffected by changes in p (Figure 4(c)), and the effects of variations in p and $Q_w(A_r)$ on profile relief are analytically decoupled.

DOI: 10.1002/esp

As shown in Figure 4(a), (b), a fourfold increase in basin-average runoff magnitude has a negligible effect on profile concavity, but produces an approximately threefold decrease in profile relief. Relief is reduced by increasing runoff because greater flow depths allow lower channel slopes to achieve the same shear stress. Note that depth increases more slowly than runoff because width also increases with discharge (Equation (9)).

The sensitivity of profile relief to variations in orographic exponent is greatest for drier conditions (low $Q_w(A_r)$) and strong orographic conditions (low p). This non-linear increase in sensitivity occurs because of a shift in the distribution of relief along the profile. When concavity is high, the elevation drop in the upstream reaches dominates the total relief. As concavity declines with decreasing orographic effect, slopes upstream of A_r are reduced while slopes downstream of A_r are increased, shifting more of the total relief to the downstream reaches. The increase in profile relief downstream of A_r is not fully compensated for by the decrease in relief upstream, because 90% of the profile length occurs downstream of A_r.

The influence of discharge on profile relief and concavity shown here results primarily from the dynamics of bedload sediment supply and transport, because we have deliberately minimized the role of bedrock incision by setting rock uplift rate and rock strength to low values in order to isolate the effects of variation in discharge. However, variations in the magnitude and spatial variation in runoff should have similar effects on steady-state profile form when significant increments in shear stress are required for incision ($\Delta\tau_E >> 0$) because of the inherent trade-off between discharge and channel slope in generating shear stress. For the remainder of this analysis we hold constant both the orographic exponent, at $p = 1{\cdot}0$, and the magnitude of discharge, at $Q_w(A_r) = 10\ m^3/s$ (which corresponds to $Q_w = 39{\cdot}1\ m^3/s$ at the S. Fork Eel River reference site (Sklar and Dietrich, 2004, 2006)). The profile concavity predicted for spatially uniform runoff, $\Theta = 0{\cdot}44$, can thus be considered a reference value for comparing the relative influence of other factors, such downstream fining or rock uplift, which we consider below.

The influence of grain size

The saltation–abrasion model suggests that the size of the coarse sediment transported as bedload has a fundamental influence on the rate of incision into bedrock (Sklar and Dietrich, 2004). Grain diameter contributes to the cover effect by influencing the threshold of motion shear stress, and to the tool effect by influencing the erosive efficiency of bedload particle impacts. Grain diameter should thus also strongly influence steady-state local channel slope (Sklar and Dietrich, 2006), and profile relief and concavity, which are the integral and spatial derivatives of local slope respectively.

Correlations between bed material grain size and channel slope have been widely noted in field studies of river longitudinal profiles (e.g. Yatsu, 1955; Miller, 1958; Rice and Church, 1998). However, a causal relationship between grain size and slope is difficult to infer in the field. For example, a given reach of an incising mountain river could be steep because the sediment grain size supplied from upstream is large, and the steep slope is required to transport the supplied coarse bedload. Conversely, the steep slope could be due to locally more resistant rock, in which case the large grains might dominate the bed of the steep reach simply because smaller grains are more easily transported through to lower slope reaches downstream. By directly coupling bedload sediment transport and bedrock incision, the saltation–abrasion model offers a mechanistic solution to this 'chicken and egg' question.

The role of grain size in influencing steady-state profile concavity and relief is most clearly isolated for conditions where the total shear stress is dominated by the threshold of motion shear stress component, as in the previous discussion of the influence of discharge. For such conditions, Figure 5(a), (b) shows the predicted variation in Θ and

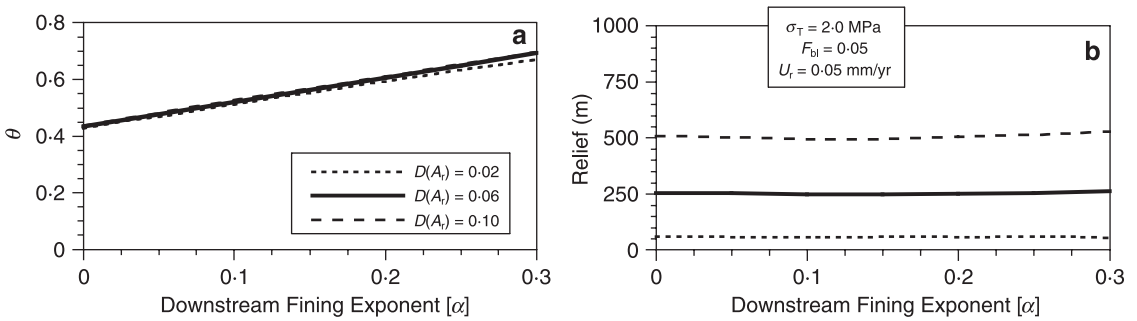

Figure 5. Influence of grain size on profile form. Variation in slope–area scaling exponent Θ (a) and profile relief (b) with changes in downstream fining exponent α, for various values of basin-average coarseness represented by the grain diameter at the representative drainage area $D_s(A_r)$.

DOI: 10.1002/esp

steady-state profile relief for a range of values of the downstream fining exponent α (Equation (11)). Variations in basin-average grain coarseness are represented by $D_s(A_r)$, the grain size at the center of the range of log-transformed drainage areas. Note that we are constrained not to vary α and $D_s(A_r)$ much more than is done here by the mechanistic assumptions underlying the model derivation (e.g. $H_w/D_s > 1{\cdot}0$), as discussed above.

The influences of downstream fining rate and average grain coarseness are distinct: downstream fining only affects profile concavity while average coarseness only affects profile relief. More rapid fining produces more concave profiles while coarser average grain sizes produce greater profile relief. This is as expected when shear stress is dominated by the threshold of motion component, which varies linearly with grain size. The influence on profile form of average grain size and the rate of downstream fining of grain size will be more complex under conditions where the other components of total shear stress ($\Delta\tau_{Qs}$ and $\Delta\tau_E$) are important, and will be considered in more detail below.

The influence of sediment supply

Under steady-state conditions, the supply rate of coarse sediment transported as bedload will depend on the rate of rock uplift, which sets the rate of sediment production, and on the partitioning of sediment between a coarse fraction that travels as bedload, and a fine fraction that travels as suspended load. This partitioning is set in the model by the parameter F_{bl}. Following the hierarchy of shear stress components discussed above, we now consider the influence of variations in sediment supply on steady-state profile form for conditions where the total shear stress is dominated by both τ_D and $\Delta\tau_{Qs}$, but not by $\Delta\tau_E$. To minimize the role of rock incision we set rock strength to a low value, hold rock uplift to a constant value and focus here on variations in sediment partitioning. The influence of variable rock uplift will be considered below.

Figure 6(a), (b) shows the variation in Θ and profile relief for values of F_{bl} ranging from 0·01 to 1·0, and for several values of average grain coarseness $D_s(A_r)$. To isolate the influence of sediment supply on profile concavity, no downstream fining occurs in this example ($\alpha = 0{\cdot}0$). Increasing sediment supply tends to reduce profile concavity and marginally increase profile relief. This occurs as $\Delta\tau_{Qs}$ makes an increasingly significant contribution to τ_T in the downstream reaches, somewhat offsetting the decline in slope that would otherwise occur due to the downstream increase in discharge. The effect is stronger for less coarse sediment grain sizes because τ_D is lower for smaller grain diameters, allowing increases in $\Delta\tau_{Qs}$ to make a relatively larger contribution to τ_T. Viewed in terms of the general downstream trend identified in the example profile (Figure 3), increases in F_{bl} and decreases in $D_s(A_r)$ tend to shift the location of the departure from threshold conditions further upstream along the profile.

The reduction in profile concavity with increasing rate of coarse sediment supply can counteract the potential increase in profile concavity due to downstream fining. Figure 7(a), (b) shows the variation in Θ and profile relief for the same range of F_{bl} as in the previous figure, now calculated for various values of the downstream fining exponent α, holding average sediment coarseness constant. As before, increasing F_{bl} reduces Θ, but now relative to the value set by downstream fining in the absence of strong influence of sediment supply. This is one of many cases where similar values of Θ may arise for widely varying conditions. For example, the profile simulations predict that $0{\cdot}4 < \Theta < 0{\cdot}5$ for each of the three combinations of the bedload partitioning and downstream fining parameters $F_{bl} \leq 0{\cdot}1$ and $\alpha = 0{\cdot}0$, $0{\cdot}2 < F_{bl} < 0{\cdot}9$ and $\alpha = 0{\cdot}15$, and $F_{bl} > 0{\cdot}7$ and $\alpha = 0{\cdot}25$.

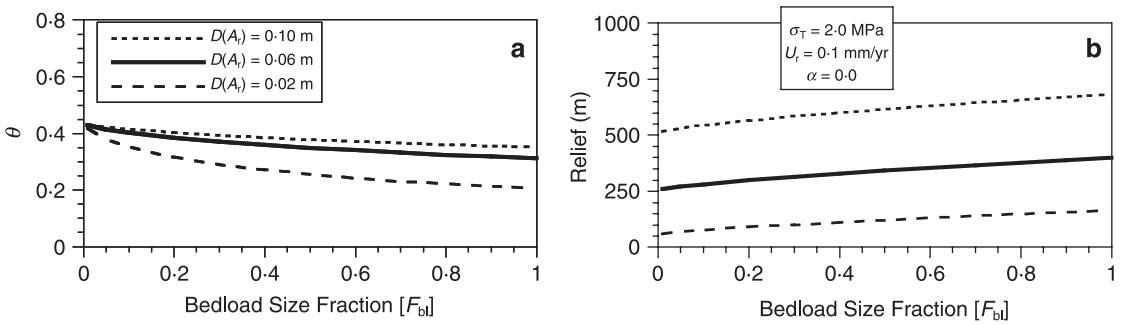

Figure 6. Influence of sediment supply rate on profile form. Variation in slope–area scaling exponent Θ (a) and profile relief (b) with changes in the fraction of total load F_{bl} occurring in the coarse bedload size class, for various values of basin-average coarseness represented by the grain diameter at the representative drainage area $D_s(A_r)$.

DOI: 10.1002/esp

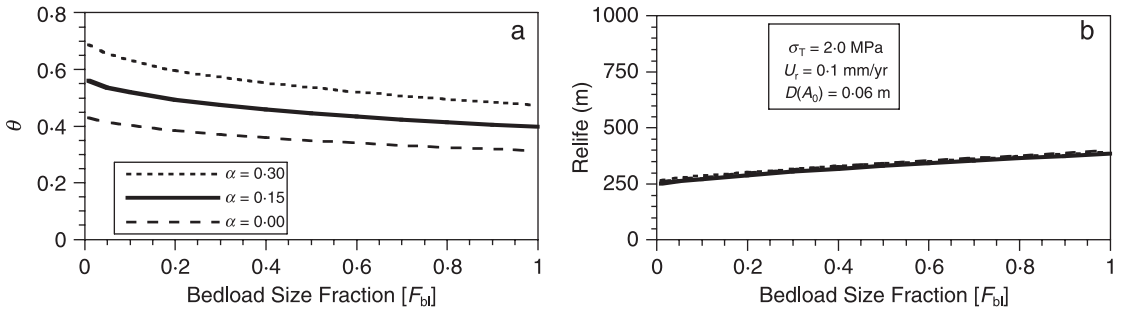

Figure 7. Offsetting influences of grain size and sediment supply on profile form. Variation in slope–area scaling exponent Θ (a) and profile relief (b) with changes in the fraction of total load F_{bl} occurring in the coarse bedload size class, for various values of the downstream fining exponent α.

The influence of rock uplift rate

Bedrock incision models based on power-law scaling arguments, such as the stream power model, implicitly assume that steady-state profile concavity is independent of rock uplift rate, and predict that profile relief scales log–log linearly with rock uplift across all possible values of rock uplift rate (see, e.g., Whipple and Tucker, 1999). More complex scaling of profile relief with rock uplift is suggested by models that include an incision threshold and account for a distribution of discharge events (see, e.g., Snyder *et al.*, 2003; Tucker, 2004). We find that the saltation–abrasion model predicts a significant influence of rock uplift rate on both profile concavity and relief, which cannot be characterized by scale-independent power law relationships.

Rock uplift rate (U_r) influences the total shear stress required to maintain steady state through its effect on both the sediment supply and the bedrock incision shear stress components $\Delta\tau_{Qs}$ and $\Delta\tau_E$. As suggested by the example profile discussed in detail above, these shear stress components contribute most to the total shear stress in the downstream reaches of the profile, particularly when downstream fining occurs. Thus, we would expect increases in rock uplift rate to reduce profile concavity by requiring greater total shear stresses, and thus steeper channel slopes, preferentially in the downstream portion of the profile.

Figure 8(a), (b) shows the predicted variation in Θ and profile relief over three orders of magnitude variation in U_r, for several values of $D_s(A_r)$. For this calculation we have held α and F_{bl} constant at moderate values, and set rock strength (σ_T) to a low value to focus on the contribution of U_r to $\Delta\tau_E$. For low values of rock uplift, both Θ and profile relief are only weakly influenced by changes in U_r. However, more rapid rates of rock uplift strongly reduce profile concavity and increase profile relief dramatically. This occurs primarily because of the increase in $\Delta\tau_{Qs}$ and secondarily because of the increase in $\Delta\tau_E$, which together gradually replace τ_D as the dominant influences on τ_T. This shift occurs first in the downstream reaches, and moves progressively upstream with increasing U_r, such that at the highest rock uplift rates only the upstream-most reaches of the profile are near threshold of motion conditions. Throughout the range of U_r, $\Delta\tau_{Qs}$ is greater than $\Delta\tau_E$, indicating that the most important effect on profile form of more rapid U_r is the increase in sediment supply. As in the previous example, the reduction in Θ with greater sediment supply (due in this

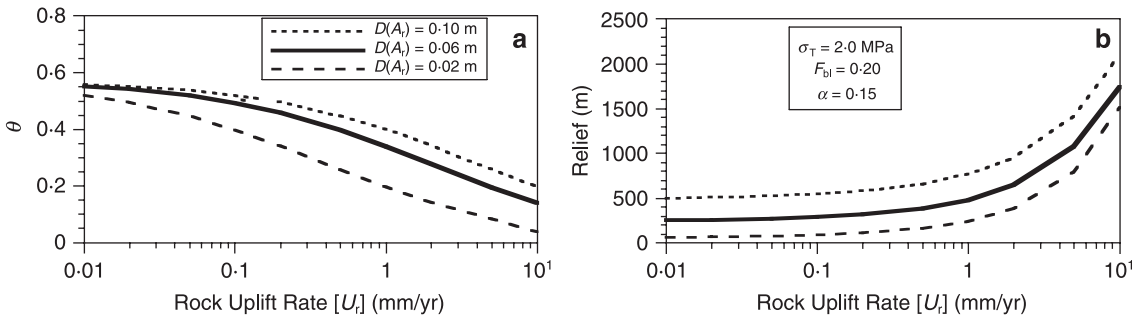

Figure 8. Influence of rock uplift rate on profile form. Variation in slope–area scaling exponent Θ (a) and profile relief (b) with changes in rock uplift rate U_r, for various values of basin-average coarseness represented by the grain diameter at the representative drainage area $D_s(A_r)$.

DOI: 10.1002/esp

case to increased U_r rather than F_{bl}) is enhanced by low values of average sediment coarseness. Similarly, variation in profile relief is roughly linear with $D_s(A_r)$, across the range of rock uplift rates.

The influence of spatial gradients on rock uplift rate

Stream power scaling models of bedrock incision, which assume a power-law dependence of incision rate on slope and drainage area, have been used to infer spatial gradients in rock uplift rate (see, e.g., Kirby and Whipple, 2001). In effect, these models assume a particular steady-state slope–area scaling and thus profile concavity for a given basin shape. Because the saltation–abrasion model predicts rather than assumes profile slope–area scaling and concavity, we can use forward modeling to explore the sensitivity of steady-state profile form to spatial gradients in rock uplift rate.

For simplicity, we assume that local rock uplift rate $U(x)$ deviates linearly from the basin-average rock uplift rate U_r, with distance away from the center of the profile length

$$\frac{U(x)}{U_r} = 1 + G\left(1 - \frac{2x}{L}\right) \tag{17}$$

where G is the dimensionless along-profile gradient in rock uplift rate, x is the distance downstream of the channel head and L is the total profile length. Figure 9(a) shows the resulting spatial pattern of local rock uplift rate for a range of positive values of G. Note that negative values of G would result in more rapid rock uplift downstream of the profile midpoint; values of $G > 1{\cdot}0$ would result in subsidence in the downstream end of the profile.

Figure 9(b), (c) shows the variation in Θ and profile relief over a range of positive values of the rock uplift gradient parameter G, for various values of sediment coarseness $D_s(A_r)$. For the case of more rapid uplift upstream of the profile midpoint, profile concavity is increased, relative to the spatially uniform uplift rate case considered above. This occurs because the increase in sediment load, and the increase in steady-state rock erosion rate, in the upstream portion of the profile require steeper channel slopes; the effect is reversed in the downstream reaches. Thus, strong gradients in rock uplift rate suppress the general downstream trend (e.g. Figure 3), in which channels shift from near threshold of motion upstream to more transport dominated conditions downstream. The enhancement of profile concavity by rock uplift gradients is strongest for finer bedload sediment supply, because, as before, local increases in $\Delta\tau_{Qs}$ are more influential for lower τ_D. Profile relief is again dominated by grain size, and is relatively insensitive to linear gradients in rock uplift rate, because increases in local channel slope upstream are offset by reductions in slope downstream.

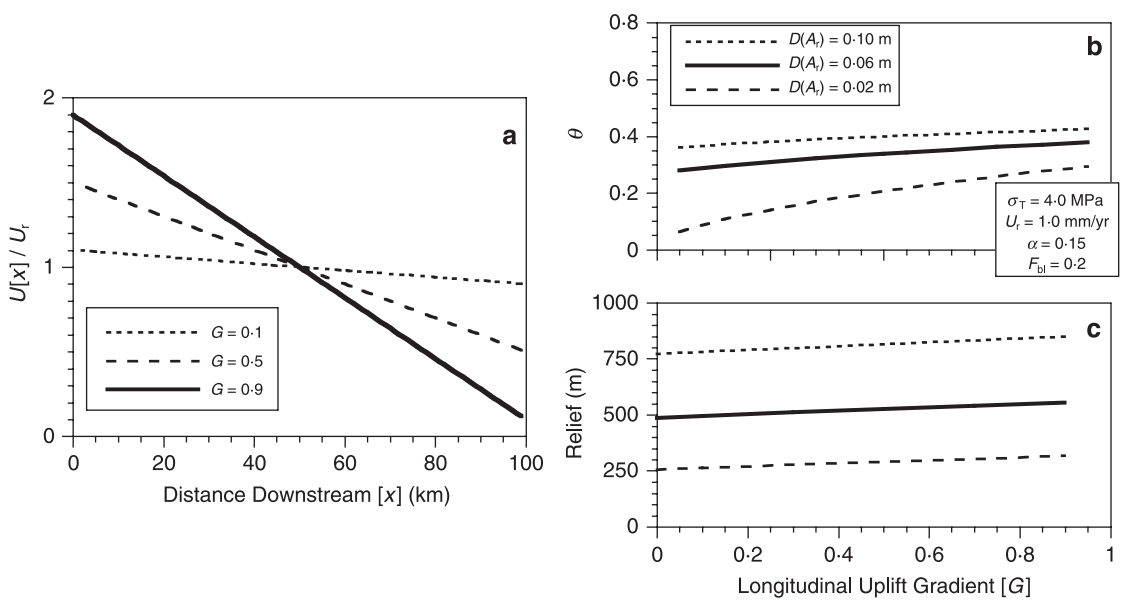

Figure 9. Influence of spatial gradients in uplift rate on profile form. (a) Variation in local rock uplift rate normalized by basin-average rock uplift rate $U(x)/U_r$ with distance upstream, for various values of the uplift gradient parameter G. Variation in slope–area scaling exponent Θ (b) and profile relief (c) with changes in uplift gradient parameter G, for various values of basin-average coarseness represented by the grain diameter at the representative drainage area $D_s(A_r)$.

DOI: 10.1002/esp

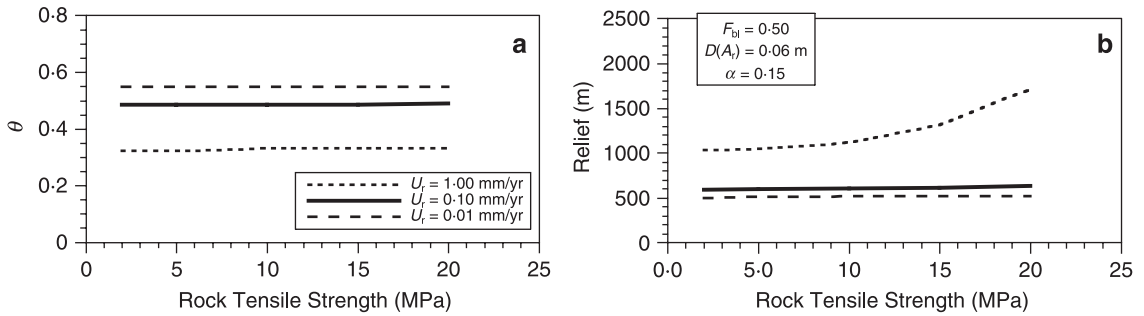

Figure 10. Influence of rock tensile strength on profile form. Variation in slope–area scaling exponent Θ (a) and profile relief (b) with changes in rock tensile strength σ_T, for various values of rock uplift rate U_r.

The influence of rock strength

Rock resistance to fluvial incision is commonly assumed to be a dominant control on steady-state channel slope, and thus on steady-state profile relief (see, e.g., Gilbert, 1877; Goldrick and Bishop, 1995). For example, the stream power bedrock incision model predicts log–log linear scaling between profile relief and the 'rock erodibility' parameter, over the full range of possible rock strengths. In contrast, the saltation–abrasion model predicts that the steady-state requirements to mobilize and transport the coarse sediment load supplied from upstream are often the dominant controls on channel slope (Sklar and Dietrich, 2006). Rock strength may be a relatively unimportant factor, except where rocks are particularly resistant and uplift rates are rapid.

Figure 10(a), (b) shows the predicted variation in Θ and profile relief with rock tensile strength σ_T, for values of rock uplift rate U_r varying by two orders of magnitude. Profile concavity is unaffected by changes in rock strength for all values of rock uplift rate simulated. Based on the example profile, which showed that the shear stress component potentially influenced by rock strength ($\Delta\tau_E$) increases in the downstream direction, we might have expected that more resistant rocks would to lead to a reduction in profile concavity, by steepening slopes preferentially in the downstream portion of the profile. However, because $\Delta\tau_E$ is always sufficiently smaller than $\Delta\tau_{Qs}$, downstream increases in $\Delta\tau_E$ do not significantly affect τ_T.

For low and moderate rock uplift rates, profile relief is also insensitive to variations in rock strength. Only when rock uplift rates are rapid does rock strength lead to increases in profile relief (Figure 10(b)). This occurs because the combination of high rock resistance and high steady-state erosion rates requires significant increases in $\Delta\tau_E$, in concert with large increases in $\Delta\tau_{Qs}$, steepening channel slopes throughout the length of the profile.

Covariation of grain size with rock uplift rate

In the sensitivity analyses discussed above we have treated as independent each of the key variables influencing bedrock incision rate and steady-state profile form. However, there may be numerous reasons to expect some systematic covariation among the key variables. For example, more rapid rates of rock uplift may produce a coarser grain size distribution in the sediments supplied to the channel network by hillslopes. This could occur because of a shift from creep to landslide dominated hillslope transport or a shift from soil mantled to bedrock hillslopes, as erosion rates increase with uplift rate at steady state. Because the absolute grain size and rate of downstream fining strongly influence profile relief and concavity respectively, as shown above, it is particularly important to investigate the effects of covariation of grain size with other key variables.

For modeling purposes, we assume a linear relationship between grain size and the logarithm of rock uplift rate:

$$D_s = 0{\cdot}06 + \beta \log\left(\frac{U_r}{0{\cdot}3}\right) \tag{18}$$

where the parameter β determines the degree of covariation, and U_r is divided by 0·3 to center the deviation from no covariance in the middle of the range of uplift rates considered here. Figure 11(a) shows the hypothesized dependence of grain size on uplift rate for three values of β. Note that the range of possible values of β is constrained by the analytical requirement that grain diameter not exceed water depth ($H_w/D_s > 1{\cdot}0$).

Figure 11(b), (c) shows the predicted variation in Θ and profile relief with rock uplift, for various values of β. For strong covariance (large β), the effects of rapid uplift rate on profile form shown previously are somewhat subdued.

DOI: 10.1002/esp

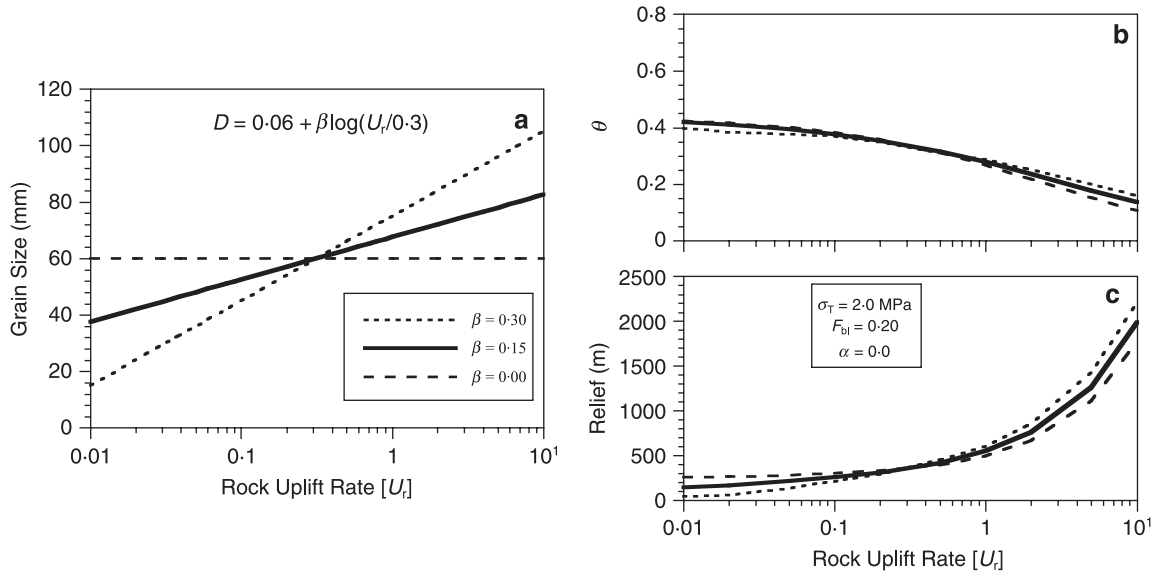

Figure 11. Covariation of grain size with rock uplift rate. (a) Assumed log–log linear variation in grain size D_s with rock uplift rate U_r for various values of the covariance parameter β. Variation in slope–area scaling exponent Θ (b) and profile relief (c) with changes in rock uplift rate U_r, for various values of the covariance parameter β.

Profile concavity is marginally greater at high uplift rates because the larger grain size increases τ_D, somewhat offsetting the increase in $\Delta\tau_{Qs}$ caused by larger steady-state sediment supply. Similarly, profile relief is marginally enhanced at high rock uplift rates, for strong covariance of grain size with uplift, because greater values of τ_D require steeper slopes. At low uplift rates, profile relief is significantly reduced by strong covariance. This is because low uplift rate produces low steady-state sediment supply, pushing channels toward the threshold of motion condition where changes in grain size will have the largest effect.

We have so far treated grain size and the fraction of total load in the bedload size class (F_{bl}) as independent. However, a coarser grain size distribution supplied to the channel network will likely lead to a greater fraction of the total load moving as bedload. To explore the effect of this potential covariation between D_s and F_{bl} on steady-state profile form, we use an expression that produces a continuous shift between two end member values, $F_{bl\text{-}max}$ and $F_{bl\text{-}min}$,

$$F_{bl} = F_{bl\text{-}max} + \frac{(F_{bl\text{-}min} - F_{bl\text{-}max})}{(1 + e^{\lambda(D_s - 0{\cdot}06)})} \tag{19}$$

where e is the base of natural logarithms, the parameter λ determines the range of D_s over which the shift occurs and the difference $(D_s - 0{\cdot}06)$ is used to center the shift in the middle of the range of grain diameters. This relationship is plotted in Figure 12(a) for three scenarios involving high, low and no covariation between F_{bl} and D_s.

The effect of covariation between F_{bl} and D_s on steady-state profile form is shown in Figure 12(b), (c), where we have plotted the variation in Θ and profile relief with the downstream fining exponent α for the three scenarios. The increase in profile concavity with increasing rate of downstream fining is substantially augmented in the high covariance scenario, compared with no covariance between F_{bl} and D_s. This is because the downstream reduction in grain size, which reduces τ_D, is accompanied by a downstream reduction in F_{bl}, which reduces the rate of increase of $\Delta\tau_{Qs}$. Thus, channel slopes decline downstream more rapidly than would be the case for a constant F_{bl} along the profile. Moreover, because downstream slopes are less steep, the overall profile relief is reduced for the high covariance scenario. Both of these effects, the increase in concavity and reduction in relief, are strongest when downstream fining is most rapid.

We now combine the two previous situations, and consider the case where D_s covaries with uplift rate and F_{bl} covaries with D_s. Here we define the high, low and no covariation scenarios as the combination of the individual high, low and no covariance scenarios from the previous examples, and hold α constant at a moderate value. Figure 13(a), (b) shows the predicted variation in Θ and profile relief with uplift for the three scenarios. For moderate to high uplift rates, the combined covariation effects lead to an increase in concavity, but very little change in profile relief. These results are not surprising, given that each of the covariation effects alone tend to increase concavity but have opposing influences on profile relief.

DOI: 10.1002/esp

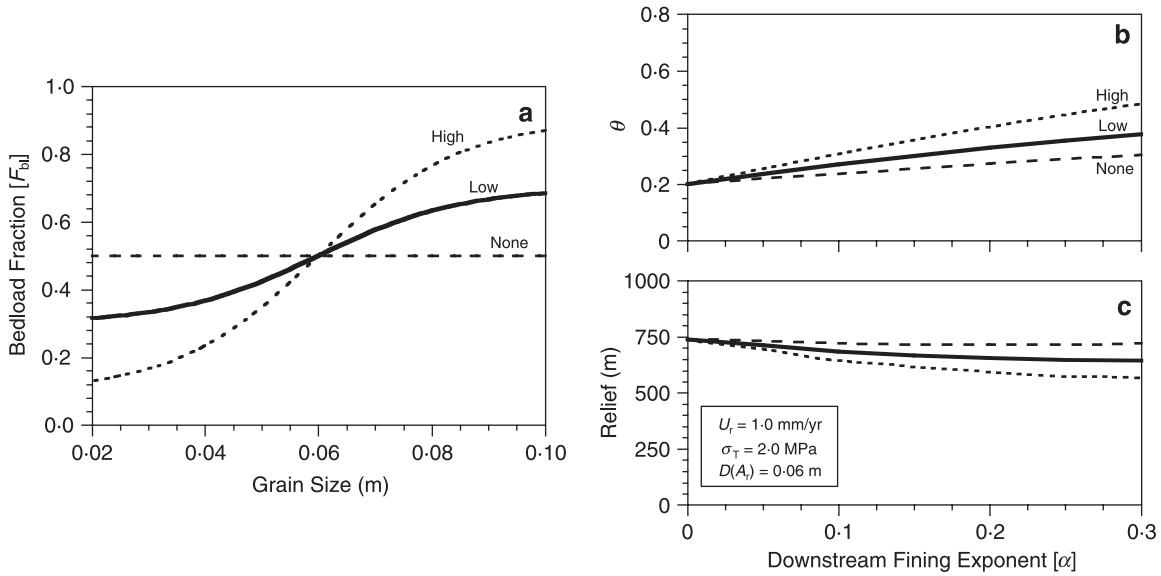

Figure 12. Covariance of bedload fraction of total load with grain size. (a) Assumed dependence of bedload fraction on grain size, for various strengths of dependence. Variation in slope–area scaling exponent Θ (b) and profile relief (c) with changes in downstream fining exponent α, for various strengths of dependence of F_{bl} on D_s.

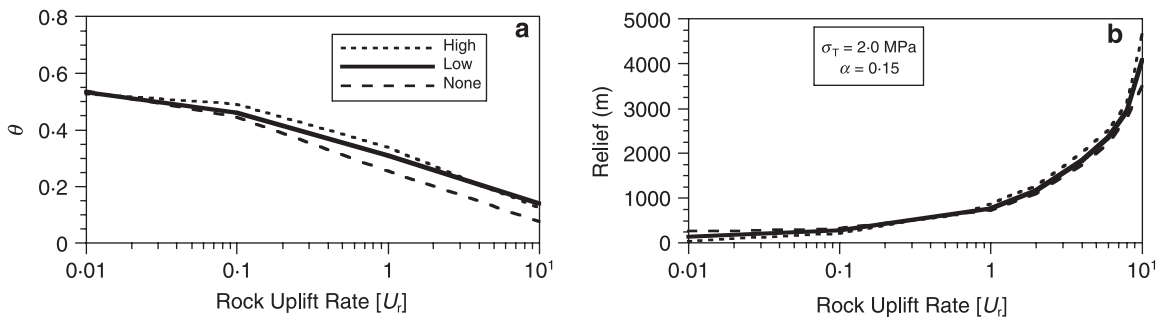

Figure 13. Combined covariance of grain size with rock uplift rate and bedload fraction with grain size. Variation in slope–area scaling exponent Θ (a) and profile relief (b) with changes in rock uplift rate, for various strengths of combined covariance.

Covariation of grain size with rock strength

The grain size of coarse sediments supplied to the channel network by hillslopes may also vary systematically with rock strength. We hypothesize that more resistant lithologies should produce coarser sediments, all else equal. For example, tree throw produces rock fragments and mixes soils vertically. For a given tree size and root strength we would expect a greater extent of rock fracturing and production of smaller rock fragments when trees rip up weaker rocks. Following the experimental observation that rock resistance to abrasive wear scales as the square of rock tensile strength σ_T (Sklar and Dietrich, 2001), we express D_s as a linear function of σ_T^2

$$D_s = 0{\cdot}05 + N(\sigma_T^2 - 100) \tag{20}$$

where the parameter N determines the strength of covariation, and the difference $(\sigma_T^2 - 100)$ is used to center the variation in D_s in the middle of the range of rock tensile strengths. This relationship is plotted in Figure 14(a). As before, we constrain the possible range of grain sizes considered to avoid the condition where $D_s > H_w$.

Figure 14(b), (c) shows the predicted variation in Θ and profile relief with rock tensile strength, for various values of N. Covariation of D_s with σ_T^2 results in a weak dependence of concavity on rock strength, but a strong influence of

DOI: 10.1002/esp

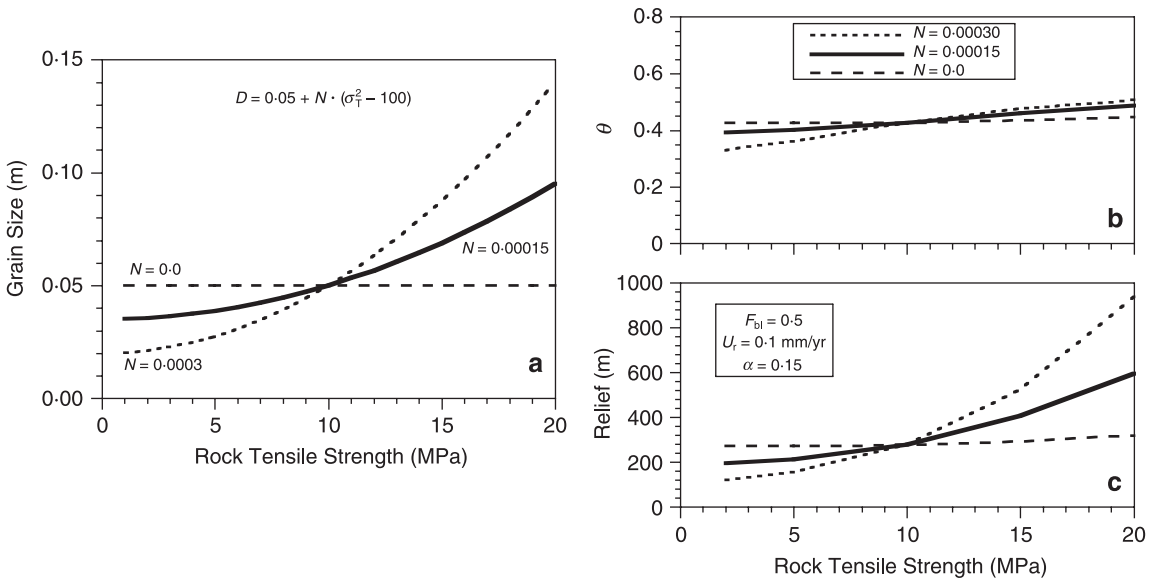

Figure 14. Covariance of grain size with rock tensile strength. (a) Assumed dependence of grain size on rock tensile strength, for various values of the covariance parameter *N*. Variation in slope–area scaling exponent Θ (b) and profile relief (c) with changes in rock tensile strength σ_T, for various values of the covariance parameter *N*.

rock strength on profile relief. This is in contrast to the earlier result (Figure 10), in which variations in rock strength had no effect on concavity and only affected profile relief for high values of rock uplift rate. The increase in concavity for strong rocks and decrease in concavity for weak rocks is due to the shift in the importance of $\Delta\tau_{Qs}$ in the downstream portions of the profile, which results from changes in the average grain coarseness and thus τ_D. The effect is similar to that shown in Figure 6(a), where for constant F_{bl} decreasing grain size increases the role of $\Delta\tau_{Qs}$ in setting τ_T and thus the slope for a given discharge. The variation in profile relief with σ_T occurs simply because rock strength becomes a proxy for grain size, reproducing the result shown in Figure 6(b). Overall, it is not surprising that allowing rock strength to control grain size enhances the influence of rock strength, because, as shown in many of the previous examples, grain size exerts a strong influence on profile form.

In the final calculation of this sensitivity analysis we consider the case of combined covariance, D_s with σ_T (Equation (20)) and F_{bl} with D_s (Equation (19)). Figure 15(a), (b) shows the variation in Θ and profile relief with rock tensile strength, for the high, low and no combined covariance scenarios. Allowing F_{bl} to vary with σ_T, indirectly through D_s, has little effect on the predicted steady-state profile form, except to suppress some of the variation in concavity for the low end of the range of rock strengths.

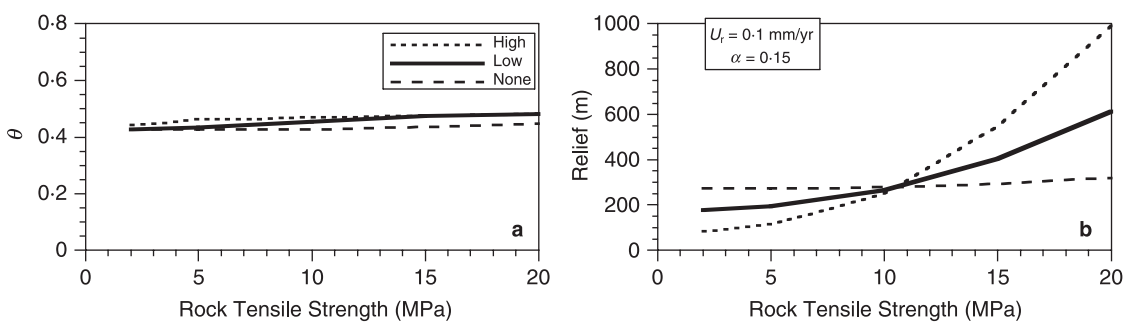

Figure 15. Combined covariance of bedload fraction with grain size and grain size with rock tensile strength. Variation in slope–area scaling exponent Θ (a) and profile relief (b) with changes in rock tensile strength σ_T, for various strengths of combined covariance.

DOI: 10.1002/esp

Discussion

The preceding analysis strongly suggests that the concavity of river longitudinal profiles, in tectonically active landscapes, results from the interplay of many variables, and cannot be said to reflect a universal slope–area scaling relationship for the process of river incision into bedrock. The common observation that slope–area scaling exponents fall into a narrow range has been cited as evidence for a simple, underlying scaling law (see, e.g., Rodriguez-Iturbe and Rinaldo, 1997). The steady-state profiles predicted by the saltation–abrasion model, however, offer a more process-specific, physically based explanation. The narrow range of Θ may occur because of the multiple influences of grain size, sediment supply and bedrock detachment, which often, but not universally, offset variations in one another. As a result, strong downstream gradients in shear stress may be rare, and the value of Θ tends to stay close to that set by the tradeoff between slope and flow depth for approximately constant shear stress (Figure 4(a)). This is illustrated in the example profile examined in detail above (Figure 2), where downstream fining, which would otherwise increase concavity, is offset by the downstream increase in sediment supply, which tends to reduce concavity. Tradeoffs between grain size and supply have been recognized previously in modeling of alluvial river profile concavity (see, e.g., Snow and Slingerland, 1987), so it is not surprising that the saltation abrasion model predicts similar dynamics in actively incising bedrock rivers.

These results imply that there may be less information about landscape forming processes and rates to be gleaned from slope–area regressions than has previously been assumed (e.g. Kirby and Whipple, 2001). Slope–area scaling cannot reveal whether a landscape is in topographic steady state (Hack, 1965; Sklar and Dietrich, 1998), and in the absence of additional information may be a poor tool for inferring rates of rock uplift. Some of the information necessary to understand profile concavity in a given landscape may be relatively easy to acquire, such as precipitation rates and their spatial gradients. Other key variables, however, are much more difficult to measure, such as the representative grain size and downstream fining rate (e.g. Attal and Lave, 2006), the fraction of the total load in the bedload size class, and rock uplift rates and their spatial gradients. Moreover, contemporary measurements of these quantities may not be adequate, because the profile form is created over a relatively long timescale and, for example, may reflect multiple climatic regimes and past exhumation of other bedrock lithologies (see, e.g., Schlunegger *et al.*, 2001).

The sensitivity analysis conducted here is clearly not exhaustive, given the large number of variables and possible interactions among them. However, unlike other model studies of profile form (e.g. Howard, 1998; Stock and Montgomery, 1999; Snyder *et al.*, 2000; van der Beek and Bishop, 2003), this analysis is based on a model of bedrock incision that has no freely adjustable parameters. Although we use simple power-law correlations in scaling up to the spatial and temporal scale of landscape evolution, each parameter has an explicit physical meaning that can be calibrated independently of the model. As a result, the quantitative predictions of profile relief and concavity calculated with the saltation–abrasion model are physically meaningful as well. We can not only make inferences about the relative importance of the key variables analyzed, but we can assess directly the fundamental scale introduced by the grain size-dependent threshold of motion. Just as the threshold of channel initiation introduces a fundamental scaling constraint on the form of hillslopes and channel networks (Dietrich and Montgomery, 1998), grain size is a fundamental constraint on profile concavity and relief, controlling, for example, the minimum channel slope and the upstream extent of what can be considered fluvial processes.

The upstream end of the model profile provides a boundary condition with more influence on profile form than has commonly been appreciated. Previously, we have shown that the steady-state relief of profiles predicted by the stream power model and other simple incision rules can be highly sensitive to the values chosen for the parameters A_0 (the unchanneled drainage area) and the slope–area scaling exponent Θ (Sklar and Dietrich, 1998). In the profile simulations reported here, the saltation–abrasion model introduces additional mechanistic constraints on the upstream profile boundary. As illustrated by the example steady-state profile (Figure 2), the saltation–abrasion model predicts that profile headwaters will typically be very close to the threshold of motion, with a downstream increase in transport stage. Because the upstream-most portion of the profile is where grain size and channel slope are greatest, and discharge and thus flow depth are least, this is where the constraint that flow depth must be greater than grain diameter is first encountered. This constraint arises because we assume that bedload transport capacity expressions (e.g. Equation (6)), and other descriptions of fluvial processes, based on the average boundary shear stress τ_T, do not apply when $H_w < D_s$ (Wiberg and Smith, 1987). Maintaining $H_w > D_s$ limits the range of combinations of D_s, α, F_t and other variable and parameter values for which steady state can be achieved. This model result is consistent with observations of headwater channels in the field, where steep ($S \geq 0{\cdot}05$), boulder dominated channels frequently occur for small drainage areas $A \approx 1$ km^2. In such channels, other models are needed to represent the effects of boulders on roughness and sediment transport (see, e.g., Buffington and Montgomery, 1999; Yager *et al.*, 2007), and to represent other incision process, such as scour by debris flows (Stock and Dietrich, 2003; Stock *et al.*, 2005).

Another important constraint on model steady-state profiles arises from the prediction of the saltation–abrasion model that there exists an absolute limit to the rate of bedrock incision by bedload abrasion (Sklar and Dietrich, 2004).

DOI: 10.1002/esp

This limit occurs because, with increasing excess shear stress, saltation hop trajectories become elongated and particle impact frequency declines more rapidly than impact energy increases, thus limiting the efficiency of the abrasion process. For a given discharge, sediment supply, grain size and rock strength, there is thus a slope that produces the maximum possible incision rate; steeper slopes will produce less rapid incision rates. If the maximum incision rate is less than the rate of rock uplift, then steady state cannot be achieved throughout the profile. As suggested by the example steady-state profile, the upstream boundary is the first place on the profile where this inability to achieve steady state will occur (Figure 3). In the simulations reported here, we have therefore limited the range of variable and parameter values to maintain steady state at the upstream profile boundary. This profile instability is suppressed by larger values of D_s and F_{bl}, and enhanced by larger values of U_r and σ_T.

In dynamic profile simulations using the saltation–abrasion model, the existence of a maximum possible incision rate leads to an instability in profile evolution. When the slope of a reach of the model channel becomes too steep, such that further increases in slope reduce, rather than increase, the predicted incision rate (Sklar and Dietrich, 2004, Figure 18 therein), a runaway increase in slope can occur, forming a model knickpoint. Because no other incision process is being modeled here, the knickpoint does not migrate, and for steady-state relative base level lowering the knickpoint can grow infinitely large.

This model result is also consistent with the field observation that other incisional processes, such as debris flow scour, may dominate in steep headwater channels (see, e.g., Seidl and Dietrich, 1992; Stock and Dietrich, 2003). The unexpected instability of the saltation–abrasion model, a property shared with some other incision models that also include the tools and cover effects (Sklar and Dietrich, 2006), leads to a set of hypotheses that can be tested in the field. First, it suggests that knickpoints may form in the absence of any structural or lithologic heterogeneities, due to an erosional instability inherent to the process of bedrock incision by bedload abrasion. Second, because this instability is more likely to occur when rock uplift rates are more rapid, or where rocks are more resistant, we would expect that knickpoint formation and upstream migration, with associated erosional mechanisms such as plunge pool scour and block-toppling (Young, 1985), might make a larger contribution to long-term rates of bedrock incision under these conditions. Third, we would expect to find more frequent, larger or more rapidly migrating knickpoints in the steeper and farther-upstream portions of river networks than in lower-gradient downstream reaches. These predictions are consistent with recent field studies (Brocard and van der Beek, 2006; Goldrick and Bishop, 2007; Crosby and Whipple, 2006; Wobus *et al.*, 2006a), which show that small drainage area and more resistant lithology correlate with the frequent occurrence of knickpoints and fluvial hanging valleys at tributary junctions.

The saltation–abrasion model also has important implications for understanding the formation of strath terraces, which are often seen as recording changes in climate or rates of rock uplift (see, e.g., Merritts *et al.*, 1994). However, strath terraces could result from the inherent variability in sediment delivery to the channel within a stable climatic and tectonic regime. Widening of river valley bottoms by lateral incision is favored by the total alluviation of the channel bed and a temporary hiatus in vertical incision, as might occur along a channel reach subjected to a pulse of elevated coarse sediment supply. A positive feedback may exist, in which lateral incision into the base of long hillslopes accelerates local sediment delivery, prolonging the period of arrested vertical incision and allowing further lateral incision to occur. Other positive feedbacks may occur because rivers that can spill across wide valley bottoms at high discharge will have less capacity to transport coarse sediment than confined channels, and because increased sinuosity reduces channel slope and increases form drag. Thus, widening channels may act as local sediment traps for periods of time long enough to effect significant lateral incision. Prolonged cessation of vertical incision will eventually create a steep knickpoint at the downstream end of the widening reach because of continuing incision in the reach immediately downstream. Terrace formation occurs when the knickpoint migrates upstream, allowing vertical incision to resume by stripping away the alluvial cover from a narrow fraction of the valley width. Finally, this scenario for strath terrace formation illustrates how knickpoints may emerge spontaneously along river profiles due to both the episodic delivery of coarse sediment and the instability inherent in the mechanics of bedrock incision by bedload abrasion discussed above.

Although we considered only steady-state profiles here, inferences can be made about aspects of transient evolution of river profiles, such as the timescale of profile adjustment to changes in rock uplift rate. The characteristic timescale (Howard, 1982) of profile adjustment, in shifting from one steady state to another, should depend in part on the extent of change in relief that results. Therefore, the sensitivity of profile relief to rock uplift rate, which we have used the saltation–abrasion model to explore, should be a proxy for the transient adjustment time. For example, as shown in Figure 11, predicted profile relief is more variable for low uplift rates when we include a dependence of grain size on uplift rate, but for high uplift rates the covariance with grain size has the opposite effect and reduces profile sensitivity.

Numerous opportunities exist to improve upon the profile analysis reported here. For example, spatially uniform, block uplift is a poor representation of tectonic boundary conditions for landscapes at nearly all spatial scales. Crustal strain is distributed over systems of multiple faults (Davis and Reynolds, 1996), typically includes flexure and other

DOI: 10.1002/esp

non-uniform patterns of motion (Stephenson, 1984) and, importantly, is dominated in convergent orogens by the horizontal motion of rock (Willett, 1999). We have also neglected the potential for feedbacks between topography and the boundary conditions that drive uplift and erosion, such as the linkages between relief and orography (Roe *et al.*, 2002), and the possible influence that surface erosion has on the path, and thus metamorphic grade, of rocks as they are incorporated into orogens and exhumed (Willet, 1999). Metamorphic grade, in turn, may influence many of the key incision variables investigated here, such as σ_T, D_s and F_{bl}. Several recent studies suggest that channel width may vary inversely with erosion rate (e.g. Harbor, 1998; Lavé and Avouac, 2000; Turowski *et al.*, 2006; Wobus *et al.*, 2006b), providing another fruitful avenue for future profile modeling. Finally, as we have noted previously, the saltation–abrasion model could be improved by explicitly representing the full distribution of grain sizes supplied to the channel network (see, e.g., Attal and Lave, 2006) as well as the full distribution of discharge and sediment supply events that drive bedrock incision (Kirkby, 1994; Tucker, 2004).

Conclusion

We have used the saltation–abrasion bedrock incision model, scaled up to the temporal and spatial scale of river longitudinal profile evolution, to explore the controls on steady-state profile relief and concavity. Profile concavity is represented by the scaling between channel slope and drainage area. A number of key results emerge, which constitute hypotheses that can be investigated in the field.

(1) During the high flow events that move bedload and incise into bedrock, steady-state profiles will tend to be close to the threshold of sediment motion in the upstream portions, with a progressive increase in transport stage in the downstream direction. The model predicts a similar downstream trend in the extent of bedrock exposure in the channel bed, from high exposure upstream to low exposure downstream.
(2) Profile concavity results from a downstream tradeoff between increasing discharge and decreasing slope in generating the shear stress required to erode at the rate of rock uplift. Total shear stress is composed of three shear stress components, responsible for initiation of sediment motion, transport of the supplied coarse sediment load and bedrock wear, respectively. Because each shear stress component can be calculated from physically meaningful values of key variables such as grain size, rock uplift rate and rock strength, significant variations in steady-state profile concavity can be predicted. Thus, we find that there is no universal slope–area scaling relationship 'intrinsic' to the process of river incision into bedrock.
(3) Profile concavity is most sensitive to spatial gradients in runoff and the rate of downstream fining of coarse sediment sizes. Concavity is also sensitive to the supply rate of coarse sediment, which varies with rock uplift rate and with the fraction of the total sediment load in the bedload size class. Variations in rock strength have little direct influence on profile concavity.
(4) Profile relief is most sensitive to the size of coarse sediments and amount of runoff, as represented by the grain diameter and discharge at a representative location along the profile. Rock uplift rate and rock strength influence relief most strongly for high rates of rock uplift.
(5) Possible covariance of grain size with rock uplift rate and rock strength suggests that the influence of these variables on profile form may occur in large part through their influence on the grain size of sediments supplied by hillslopes to channels. Similarly, covariance between grain size and the fraction of sediment load in the bedload size class provides another indirect avenue for rock uplift and strength to influence profile form.
(6) The narrow range of values of the slope–area scaling exponent commonly observed in the field may result from the offsetting influences on profile concavity of the key variables, as might occur when the reduction in concavity due to high rock uplift rate is counteracted by rapid downstream fining of grain size.
(7) Knickpoints may spontaneously emerge in the river profile due to an instability created by an inherent limit to the erosional efficiency of saltating bedload, without any influence by structural or lithologic heterogeneities. Frequency of knickpoint occurrence, and magnitude of knickpoint height and upstream migration rate, are favored by more rapid rates of rock uplift and by more resistant rock, and by proximity to the upstream profile boundary.

Acknowledgements

We thank G. Hauer, A. Howard, J. Kirchner, A. Luers, J. Roering, M. Stacey, J. Stock and K. Whipple for provocative and insightful discussions, and P. Bishop, P. van der Beek and G. Tucker for thoughtful review comments that helped improve the manuscript. This research was supported in part by the STC program of the National Science Foundation (NSF) via the National Center for Earth Surface Dynamics (NCED) under agreement EAR-0120914, and by NSF grants EAR-970608 and EAR-0345344.

DOI: 10.1002/esp

References

Abbott JE, Francis JRD. 1977. Saltation and suspension trajectories of solid grains in a water stream. *Philosophical Transactions of the Royal Society, London, Series A* **284**: 225–254.

Ahnert F. 1970. Functional relationships between denudation, relief, and uplift in large mid-latitude drainage basins. *American Journal of Science* **268**: 243–463.

Attal M, Lave J. 2006. Changes of bedload characteristics along the Marsyandi river (central Nepal): implications for understanding hillslope sediment supply, sediment load evolution along fluvial networks, and denudation in active orogenic belts. In *Tectonics, Climate and Landscape Evolution*, Geological Society of America Special Paper 398, Penrose Conference Series, Willett SD, Hovius N, Brandon MT, Fisher DM (eds); 143–171. DOI: 10.1130/2006.2398(09)

Bevin KJ. 1996. Equifinality and uncertainty in geomorphic modeling. In *The Scientific Nature of Geomorphology*, Rhoads BL, Thorn CE (eds). Wiley: New York; 289–313.

Bitter JGA. 1963. A study of erosion phenomena, part I. *Wear* **6**: 5–21.

Brocard GY, van der Beek PA. 2006. Influence of incision rate, rock strength and bedload supply on bedrock river gradients and valley-flat widths: field-based evidence and calibrations from western Alpine rivers (SE France). In *Tectonics, Climate and Landscape Evolution*, Geological Society of America Special Paper 398, Penrose Conference Series, Willett SD, Hovius N, Brandon MT, Fisher DM (eds); 127–141. DOI: 10.1130/2006.2398(07)

Brush LM. 1961. *Drainage Basins, Channels, and Flow Characteristics of Selected Streams in Central Pennsylvania*, US Geological Survey Professional Paper 282-F.

Buffington JM, Montgomery DR. 1999. Effects of hydraulic roughness on surface textures of gravel-bed rivers. *Water Resources Research* **35**: 3507–3522.

Crosby B, Whipple KX. 2006. Knickpoint initiation and distribution within fluvial networks: 236 waterfalls in the Waipaoa River, North Island, New Zealand. *Geomorphology* **82**: 16–38. DOI: 10.1016/j.geomorph.2005.08.023

Davis GH, Reynolds SJ. 1996. *Structural Geology of Rocks and Regions*. Wiley: New York.

Dietrich WE, Montgomery DR. 1998. Hillslopes, channels, and landscape scale. In *Scale Dependence and Scale Invariance in Hydrology*, Sposito G (ed.). Cambridge University Press: Cambridge; 30–60.

Fernandez-Luque R, van Beek R. 1976. Erosion and transport of bed-load sediment. *Journal of Hydraulic Research* **14**: 127–144.

Flint JJ. 1974. Stream gradient as a function of order, magnitude and discharge. *Water Resources Research* **10**: 969–973.

Gasparini NM, Bras RL, Whipple KX. 2006. Numerical modeling of non-steady-state river profile evolution using a sediment-flux-dependent incision model. In *Tectonics, Climate and Landscape Evolution*, Geological Society of America Special Paper 398, Penrose Conference Series, Willett SD, Hovius N, Brandon MT, Fisher DM (eds); 127–141. DOI: 10.1130/2006.2398(08)

Gilbert GK. 1877. *Report of the Geology of the Henry Mountains, Geographical and Geological Survey of the Rocky Mountain Region*. Government Printing Office: Washington, DC.

Goldrick G, Bishop P. 1995. Differentiating the roles of lithology and uplift in the steepening of bedrock river long profiles: an example from Southeastern Australia. *Journal of Geology* **103**: 227–231.

Goldrick G, Bishop P. 2007. Regional analysis of bedrock stream long profiles: evaluation of Hack's SL form, and formulation and assessment of an alternative (the DS form). *Earth Surface Processes and Landforms* **32**: 649–671. DOI: 10.1002/esp.1413

Gomez B, Church M. 1989. An assessment of bedload sediment transport formulae for gravel-bed rivers. *Water Resources Research* **25**: 1161–1186.

Hack JT. 1957. *Studies of Longitudinal Stream Profiles in Virginia and Maryland*, US Geological Survey Professional Paper 294-B.

Hack JT. 1965. *Postglacial Drainage Evolution and Stream Geometry in the Ontonagon Area, Michigan*, US Geological Survey Professional Paper P-0504-B.

Hancock GR, Willgoose GR. 2002. The use of a landscape simulator in the validation of the Siberia landscape evolution model: transient landforms. *Earth Surface Processes and Landforms* **27**: 1321–1334.

Harbor DJ. 1998. Dynamic equilibrium between an active uplift and the Sevier River, Utah. *Journal of Geology* **106**: 181–194.

Head WJ, Harr ME. 1970. The development of a model to predict the erosion of materials by natural contaminants. *Wear* **15**: 1–46.

Howard AD. 1982. Equilibrium and time scales in geomorphology: application to sand-bedded alluvial streams. *Earth Surface Processes and Landforms* **7**: 303–325.

Howard AD. 1994. A detachment-limited model of drainage basin evolution. *Water Resources Research* **30**: 2261–2286.

Howard AD. 1998. Long profile development of bedrock channels: interaction of weathering, mass wasting, bed erosion, and sediment transport. In *Rivers Over Rock: Fluvial Processes in Bedrock Channels*, American Geophysical Union Geophysical Monograph Series 107, Tinkler K, Wohl EE (eds); 297–319.

Howard AD, Dietrich WE, Seidl MA. 1994. Modeling fluvial erosion on regional to continental scales. *Journal of Geophysical Research* **99**(B7): 13 971–13 986.

Howard AD, Kerby G. 1983. Channel changes in badlands. *Geological Society of America Bulletin* **94**: 739–752.

Hu C, Hui Y. 1996. Bed-load transport I: Mechanical characteristics. *Journal of Hydraulic Engineering* **122**: 245–254.

Kirby E, Whipple K. 2001. Quantifying differential rock-uplift rates via stream profile analysis. *Geology* **29**: 415–418.

Kirkby MJ. 1994. Thresholds and instability in stream head hollows: a model of magnitude and frequency for wash processes. In *Process Models and Theoretical Geomorphology*, Kirkby MJ (ed.). Wiley: New York; 295–314.

Kooi H, Beaumont C. 1996. Large-scale geomorphology: classical concepts reconciled and integrated with contemporary ideas via a surface processes model. *Journal of Geophysical Research* **101**(B2): 3361–3386.

Lavé J, Avouac JP. 2000. Active folding of fluvial terraces across the Siwaliks Hills (Himalayas of central Nepal). *Journal of Geophysical Research* **105**: 5735–5770.

Mackin JH. 1948. Concept of the graded river. *Bulletin of the Geological Society of America* **59**: 463–512.

Merritts DJ, Vincent KR, Wohl EE. 1994. Long river profiles, tectonism, and eustasy: a guide to interpreting fluvial terraces. *Journal of Geophysical Research* **99**(B7): 14031–14050.

Miller JP. 1958. *High Mountain Streams: Effects of Geology on Channel Characteristics and Bed Material*, New Mexico State Bureau of Mines and Mineral Resources, Memoir 4.

Molnar P. 2001. Climate change, flooding in arid environments, and erosion rates. *Geology* **29**(12): 1071–1074. DOI: 10.1130/0091-7613

Molnar P, England P. 1990. Late Cenozoic uplift of mountain ranges and global climate change: chicken or egg? *Nature* **346**: 29–34.

Montgomery DR, Foufoula-Georgiou E. 1993. Channel network source representation using digital elevation models. *Water Resources Research* **29**: 3925–3934.

Montgomery DR, Lopez-Blanco J. 2003. Post-Oligocene river incision, southern Sierra Madre Occidental, Mexico. *Geomorphology* **55**: 235–247.

O'Connor JE, Costa JE. 2004. Spatial distribution of the largest rainfall-runoff floods from basins between 2.6 and 26 000 km^2 in the United States and Puerto Rico. *Water Resources Research* **40**: W01107. DOI: 10.1029/2003WR002247

Rice SP, Church M. 1998. Grain size along two gravel-bed rivers: statistical variation, spatial pattern and sedimentary links. *Earth Surface Processes and Landforms* **23**: 345–363.

Rice SP, Church M. 2001. Longitudinal profiles in simple alluvial systems. *Water Resources Research* **37**(2): 417–426.

Rodriguez-Iturbe I, Rinaldo A. 1997. *Fractal River Basins: Chance and Self-Organization*. Cambridge University Press: New York.

Roe GH, Montgomery DR, Hallet B. 2002. Effects of orographic precipitation variations on the concavity of steady-state river profiles. *Geology* **30**(2): 143–146.

Schlunegger F, Melzer J, Tucker GE. 2001. Climate, exposed source-rock lithologies, crustal uplift and surface erosion: a theoretical analysis calibrated with data from the Alps/North Alpine Foreland Basin system. *International Journal of Earth Science* **90**: 484–499.

Seidl MA, Dietrich WE. 1992. The problem of channel erosion into bedrock. In *Functional Geomorphology*, Schmidt KH, de Ploey J (eds). *Catena Supplement* **23**: 101–124.

Seidl MA, Dietrich WE, Kirchner JW. 1994. Longitudinal profile development into bedrock: an analysis of Hawaiian channels. *Journal of Geology* **102:** 457–474.

Sinha SK, Parker G. 1996. Causes of concavity in longitudinal profiles of rivers. *Water Resources Research* **32**: 1417–1428.

Sklar LS, Dietrich WE. 1998. River longitudinal profiles and bedrock incision models: stream power and the influence of sediment supply. In *Rivers Over Rock: Fluvial Processes in Bedrock Channels*, American Geophysical Union Geophysical Monograph Series 107, Tinkler K, Wohl EE (eds); 237–260.

Sklar LS, Dietrich WE. 2001. Sediment and rock strength controls on river incision into bedrock. *Geology* **29**: 1087–1090.

Sklar LS, Dietrich WE. 2004. A mechanistic model for river incision into bedrock by saltating bedload. *Water Resources Research* **40**: W06301. DOI: 10.1029/2003wr002496

Sklar LS, Dietrich WE. 2006. The role of sediment in controlling bedrock channel slope: implications of the saltation–abrasion incision model. *Geomorphology* **82**: 58–83. DOI: 10.1016/j.geomorph.2005.08.019

Sklar LS, Dietrich WE, Howard AD. 1996. The influence of sediment supply on river incision into bedrock: a theoretical investigation. *EOS, Transactions, American Geophysical Union* **77** (Fall Meeting Supplement): 46, Abstract H32A-12.

Snow RS, Slingerland RL. 1987. Mathematical modeling of graded river profiles. *Journal of Geology* **95**: 15–33.

Snyder NP, Whipple KX, Tucker GE, Merritts DJ. 2000. Landscape response to tectonic forcing: digital elevation model analysis of stream profiles in the Mendocino triple junction region, northern California. *Geological Society of America Bulletin* **112**: 1250–1263.

Snyder NP, Whipple KX, Tucker GE, Merritts DJ. 2003. Importance of a stochastic distribution of floods and erosion thresholds in the bedrock incision problem. *Journal of Geophysical Research* **108**: B2, 2117. DOI: 10.1029/2001JB001655

Stephenson R. 1984. Flexural models of continental lithosphere based on the long-term erosional decay of topography. *Geophysical Journal of the Royal Astronomical Society* **77**: 385–413.

Stock JD, Dietrich WE. 2003. Valley incision by debris flows: evidence of a topographic signature. *Water Resources Research* **39**: 1089. DOI: 10.1029/2001wr001057

Stock JD, Montgomery DR. 1999. Geologic constraints on bedrock river incision using the stream power law. *Journal of Geophysical Research* **104**: 4983–4993.

Stock JD, Montgomery DR, Collins BD, Dietrich WE, Sklar LS. 2005. Field measurements of incision rates following bedrock exposure: implications for process controls on the long profiles of valleys cut by rivers and debris flows. *Geological Society of America Bulletin* **117**(11/12): 174–194. DOI: 10.1130/B25560

Tucker GE. 2004. Drainage basin sensitivity to tectonic and climatic forcing: implications of a stochastic model for the role of entrainment and erosion thresholds. *Earth Surface Processes and Landforms* **29**: 185–205. DOI: 10.1002/esp.1020

Tucker GE, Whipple KX. 2002. Topographic outcomes predicted by stream erosion models: sensitivity analysis and intermodel comparison. *Journal of Geophysical Research* **107**(B9): 2179. DOI: 10.1029/2001JB000162

Turowski JM, Lague D, Crave A, Hovius N. 2006. Experimental channel response to tectonic uplift. *Journal of Geophysical Research* **111**: F03008. DOI: 10.1029/1002JB001655

van der Beek P, Bishop P. 2003. Cenozoic river profile development in the Upper Lachlan catchment (SE Australia) as a test of quantitative fluvial incision models. *Journal of Geophysical Research* **108**(B6): 2309. DOI: 10.1029/2002JB002125

Whipple KX. 2001. Fluvial landscape response time: how plausible is steady-state denudation? *American Journal of Science* **301**: 313–325.

Whipple KX, Tucker GE. 1999. Dynamics of the stream-power river incision model: implications for height limits of mountain ranges, landscape response timescales, and research needs. *Journal of Geophysical Research* **104B**: 17661–17674.

Whipple KX, Tucker GE. 2002. Implications of sediment-flux-dependent river incision models for landscape evolution. *Journal of Geophysical Research* **107**(B2). DOI: 10.1029/2000JB000044

Wiberg PL, Smith JD. 1987. Initial motion of coarse sediment in streams of high gradient. In *Erosion and Sedimentation in the Pacific Rim*, International Association of Hydrological Sciences Publication 165, Beschta RL (ed.); 299–308.

Willett SD. 1999. Orogeny and orography: the effects of erosion on the structure of mountain belts. *Journal of Geophysical Research* **104**: 28957–28981.

Willett SD, Brandon MT. 2002. On steady states in mountain belts. *Geology* **30**: 175–178.

Wobus CW, Crosby BT, Whipple KX. 2006a. Hanging valleys in fluvial systems: controls on occurrence and implications for landscape evolution. *Journal of Geophysical Research* **111**: F02017. DOI: 10.1029/2005JF000406

Wobus CW, Tucker GE, Anderson RS. 2006b. Self-formed bedrock channels. *Geophysical Research Letters* **33**. DOI: 10.1029/2006GL027182

Yager E, Kirchner JW, Dietrich WE. 2007. Calculating bedload transport in steep, boulder bed channels. *Water Resources Research* **43**: W07418. DOI: 10.1029/2006WR005432

Yatsu E. 1955. On the longitudinal profile of the graded river. *Transactions, American Geophysical Union* **36**(4): 211–219.

Young RW. 1985. Waterfalls: form and process. *Zeitschrift für Geomorpholgie NF* **55**: 81–85.